Spring 5-23-2019

Geomorphic and temporal evolution of a Mississippi delta flanking barrier island: Grand Isle, LA

Julie A. Torres
University of New Orleans, jatorre0@gmail.com

Geomorphic and temporal evolution of a Mississippi delta flanking barrier island: Grand Isle, LA

A Thesis

Submitted to the Graduate Faculty of the
University of New Orleans
in partial fulfillment of the
requirements for the degree of

Master of Science
in
Earth and Environmental Sciences
Coastal and Geomorphologic Studies

by

Julie Torres

B.S. University of New Orleans, 2009
B.S. University of New Orleans, 2012

May, 2019

ACKNOWLEDGEMENTS

This thesis is a work that should be considered a collaborative one, as many people helped me get to the point of conclusion, whether by way of furnishing field assistance, providing expertise, or otherwise.

GPR collection on Grand Isle was a task much more easily conquered with assistance. Thank you, Frances Crawford and Jarrett Levesh for donating some of your own precious time to join me in the field; you made the trips effortless, efficient, and definitely more fun. Field work would also not have been possible without the behind-the-scenes work of Mike Brown. Thank you, Mike, for helping me gather supplies, secure vehicles, and complete purchase orders.

Back on campus, I must have summoned Ben Beasley a dozen times to help me with technical/computer program issues. Thank you, Ben. Not once did I ever sense hesitation or reluctance from you, but only a rare and genuine willingness to help however you could.

Ms. Jenna Fischer assisted with sample preparations and data collection at NDSU. I would also like to acknowledge the support of The Ohio State University Nuclear Reactor Laboratory and the assistance of reactor staff for the neutron irradiation and gamma spectroscopy capabilities as well as Joe Talnagi of Scientific Consulting Services for INAA data reduction.

To my committee:

Mark A. Kulp: You saw progress and pioneering research when I saw none; you were particularly encouraging in this respect. After being my professor and/or advisor for nearly a decade, you've become acutely aware of my capabilities and encouraged me to push beyond them.

Ioannis Y. Georgiou: Thank you for donating you time and expertise on items of the mathematical sort. You helped me reach quite a few of those satisfying "a-ha!" moments for some of the most fundamental concepts of this research.

Duncan FitzGerald: By way of long-distance assistance, you provided your fresh perspectives and angles regarding the research with a level of excitement that rivaled my own.

Finally, working to complete original research while being ill in more ways than one was sometimes exceptionally difficult. To anyone who may have had the misfortune of bumping into me on a bad day, thank you for understanding.

This work was funded in part with the 2018 Shell Minority or Women in Science Scholarship and the New Orleans Geological Society Richard W. Boebel Graduate Scholarship received in 2017.

TABLE OF CONTENTS

LIST OF FIGURES

LIST OF TABLES

ABSTRACT

Optically stimulated luminescence (OSL) dating beach ridge sediments is one method for resolving barrier island growth at intermediate scales (decades-centuries), information that is lacking for Louisiana. This research combines OSL, GPR, aerial imagery, and cores to document temporal and spatial evolution of a Louisiana barrier island.

Grand Isle is composed of beach ridges organized in distinct, unconformable sets that began forming 0.75 ka until 0.575 ka when deposition ceased, the ridges were partially eroded, and deposition resumed in a more eastward direction. The central ridges formed between 370±30 and 170±10 years ago at a rate of one ridge every 11.6 years with sand from the eroding Caminada headland that, with flanking barriers, forms the Bayou Lafourche transgressive depositional system. Grand Isle's lithosome (92,600,000 cubic meters) requires an annual longshore transport of 128,625 cubic meters. The lithosome thickness (10 meters) and steady sediment supply stabilize the island relative to other Louisiana barriers.

Keywords: barrier evolution, beach ridge, coastal geomorphology, Mississippi river delta, OSL chronology, Louisiana coastal plain

1. INTRODUCTION

Barrier islands constitute an estimated 6.5% of the world's open-ocean coasts, 30% of which are associated with delta shorelines (Stutz & Pilkey, 2001). Barriers on the Atlantic and Gulf coasts of the United States comprise only 10% by number but 24% by length globally (Stutz & Pilkey, 2001). Barrier islands serve many functions including protecting the mainland and fragile backbarrier ecosystems during storms as well as providing unique wildlife habitats due to their exposure.

Barrier islands are classified as *retrograding* (eroding barriers migrating onshore), *aggrading* (accreting vertically as sea level rises), or *prograding* (building seaward). In a regime of slow sea level rise, prograding barriers build seaward due to an abundant sediment supply, commonly through the addition of successive beach ridges. These barriers, like Grand Isle in Louisiana, are called "beach ridge barriers." Beach ridge barriers are important for studies of coastal evolution because the ridges contain a geo-archive of coastal conditions (Scheffers et al., 2011).

Globally distributed beach ridge systems belong to the most promising geo-archives for coastal development studies (Scheffers et al., 2011). Numerous studies have shown that beach ridge sequences are useful for reconstructing environmental conditions, such as Holocene sea level variations, climate change, past storm intensities, and extreme wave events (Scheffers et al., 2011). Previous studies show that geomorphic features contained within Louisiana's barrier islands can provide important records of the character and rate of shoreline change as well as records of past sea level (Morton et al., 2000; Otvos, 2005; Rosati & Stone, 2009).

The formation of barrier islands along the Mississippi deltaic coast (Fig. 1) has been well-documented, yet the pace at which they evolve is essentially unconstrained. Penland et al. (1988), on the basis of age and geomorphologic relationships between prograded deltaic headlands and barrier shorelines, conceptualized a 3-stage process of barrier formation known as transgressive submergence (Fig. 2). In the Penland et al. (1988) model active deltaic headlands are abandoned by upstream fluvial avulsions and undergo transgressive reworking in a regime of relative sea level rise (RSLR) and sediment starvation. Marine processes winnow formerly deposited deltaic headland sediment, thereby concentrating the relatively coarser grained sediment that accumulates and is carried alongshore, forming flanking barrier islands. Barrier islands in Louisiana are intrinsically linked to abandoned deltaic lobes of the Mississippi River and subsequent reworking by littoral and inner shelf processes. Stage 1 of

the conceptual model is well-represented by the erosional remnants of the Lafourche delta defined by the Timbalier Islands, Caminada headland, and Grand Isle.

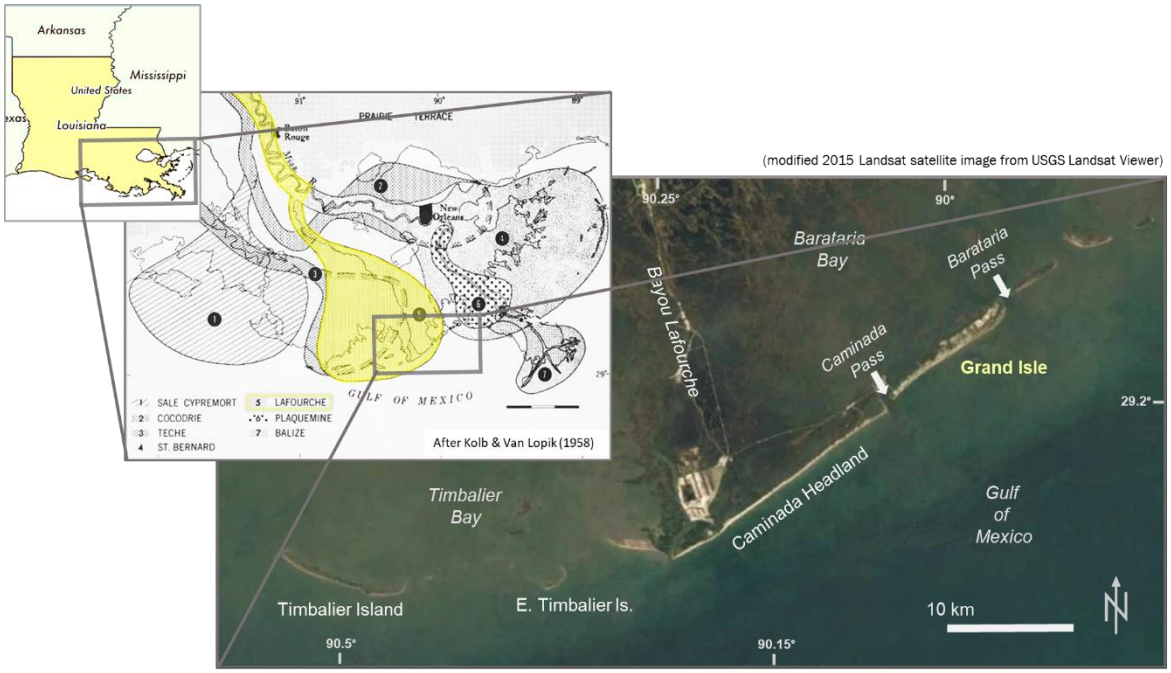

Fig. 1. Inset map of southern Louisiana showing barrier islands of south-central Louisiana and that Grand Isle is a product of erosion of the Lafourche delta complex (yellow), one deltaic complex of the Holocene Mississippi river delta plain (e.g. Kolb & Van Lopik, 1958 and many others).The Bayou Lafourche barrier system extends from Timbalier Island to Grand Isle (modified 2015 Landsat satellite image from USGS Landsat Viewer).

Despite the many previous studies of the Louisiana coast (e.g. Penland & Ramsey, 1990; Penland et al., 1985; Dokka, 2006; Kulp et al., 2005; Georgiou et al., 2010), the rate at which the flanking barrier shorelines form has not been clearly demonstrated. This study of Grand Isle is the first known use of optically stimulated luminescence (OSL) on a Louisiana barrier island beach ridge system to determine rates of flanking barrier island formation through along shore barrier progradation. Aerial imagery, well logs, OSL dating, and ground penetrating radar (GPR) surveys are used to document the stratigraphy, timing of beach ridge formation and progradation, geologic framework, and the overall evolution of

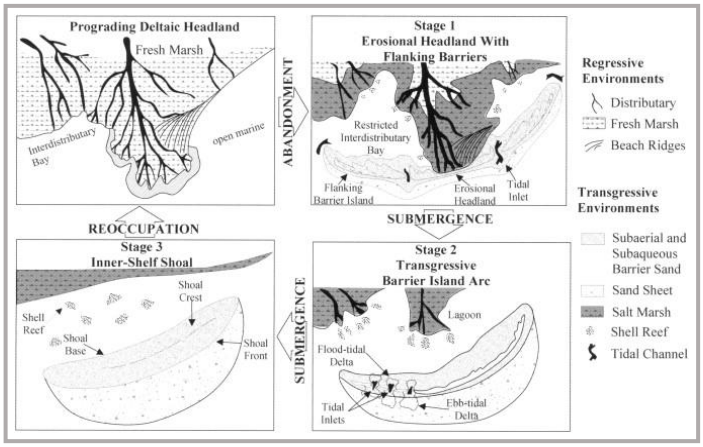

Fig. 2. Penland and Boyd (1981) defined three stages for deltaic barrier island formation and provided a depositional framework for the Mississippi River and its Holocene deltas. Penland & Boyd (1981), modified by Kulp et al. (2005).

Grand Isle. This work refines and expands the current body of knowledge about the dimensions and age of the Grand Isle barrier lithosome, provides an estimate of the sediment source and transport rates responsible for island growth, provides an evolutionary understanding for a headland-flanking barrier island of the Mississippi River delta (MRD) plain Penland et al. (1988) model, and assesses the generally stable nature of Grand Isle relative to adjacent barrier systems in the face of regional sea level rise.

2. REGIONAL SETTING

Grand Isle is located along the central coast of Louisiana and is part of the Barataria Bay barrier shoreline. The island is adjacent to the former Lafourche distributary system that forms the shallow subsurface and surface geologic framework of the eastern Terrebone and western Barataria Basins. The late, active regressive stage of the distributary is closely linked to formation of the eastern Caminada beach ridge plain (Kulp et al., 2005). The Grand Isle shoreline trends northeast approximately 11 km from the more westerly located sand-rich Caminada barrier headland; Grand Isle and Caminada headland are separated by Caminada Pass (Fig. 1). The system consists of the central erosional Caminada headland and flanking barrier islands on either side, Caminada Pass spit and Grand Isle to the east and Raccoon Pass spit and Timbalier Islands to the west. The primary sand source of these shorelines is the now transgressive Caminada beach ridge plain (Penland et al., 1986) and nourishment sand (Jafari et al., 2018). The long-term history (approximately 500 years based on shoreline erosion trends and spit development) of the Bayou Lafourche headland-Caminada beach ridge plain has been characterized by erosion of the central headland with concurrent development and lateral growth of flanking barrier islands (Penland et al., 1992).

In addition to the effects of eustatic (global) sea level rise (3.1 mm/yr; Church & White, 2011), southern Louisiana is subjected to significant subsidence (9 mm/yr; Nienhuis et al., 2017) caused by regional isostatic subsidence produced by Quaternary sediment and water loading (Jurkowski et al., 1984; Ivins et al., 2007; Syvitski et al., 2009), faulting (e.g., Kolb et al., 1975; Dokka, 2006; Dokka et al., 2006), sediment compaction (Penland & Ramsey, 1990; Edrington et al., 2008), and groundwater pumping (Kazmann & Heath, 1968). The average shoreline change of the Lafourche Delta during the past century has been -11 m/yr (Martinez et al., 2009), whereas Grand Isle has experienced a net positive rate of shoreline change along the east end (0.55 m/yr). Rather than migrating landward, as is typical for barriers along the Louisiana coast, Grand Isle has slowly rotated clockwise around a stable midpoint (McBride et al., 1995; McBride & Byrnes, 1997).

The beach at Grand Isle is backed by an active dune system that in some cases, where abundant sand is available, has accreted on top of a hurricane surge protection levee. Farther inland numerous low ridges separated by low elevation swales are nearly aligned parallel to the modern beach shoreline. The ridges were first described by Conatser (1971) who identified 25 to 35 northeast-trending ridges with spacings of 15 to 150 m and elevations from 0.1 to 1.0 m high.

3. METHODS

3.1 Beach ridge mapping and geometric analysis

On the basis of 1956 direct-overhead aerial photography, Conatser (1971) identified approximately 15 complete, continuous northeast-trending ridges consisting of a shore-parallel segment and a more lagoonward recurved segment. Also identified were at least 30 shorter**,** truncated ridge segments. Ninety additional ridges and 10 ridge sets were identified as part of this study using higher-resolution 1965 aerial imagery (Fig. 3). A series of three 1956 photographs were carefully stitched together and georeferenced in Geographic Information Software (GIS) software.

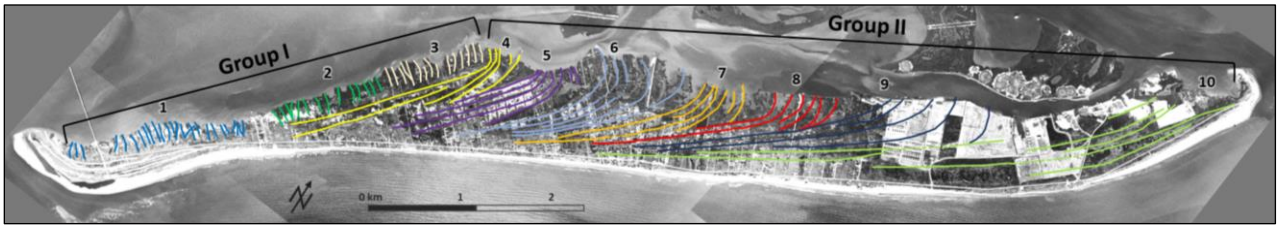

Fig. 3. Beach ridges mapped in this study using 1956 aerial imagery, split into two groups and smaller sets based on truncations and significant differences in ridge bearing and spacing.

The ridges exhibit slight relief (<1 m) in the center of the island and negligible relief (10's of cm's) elsewhere; therefore, changes in elevation provide only a secondary indication of beach ridge locations. The primary indicators of beach ridge presence are large trees that grow in narrow strips with an along island-strike elongated axis and are clearly visible in the aerial photography. Ridges identified in the imagery were divided into primary groups (Groups I and II) and secondary sets (1-9); these distinctions were based on individual ridge morphological characteristics such as orientation, curvature, and truncations or sharp unconformities.

Once the ridge groups and sets were mapped, the spacing between adjacent ridges was measured using the *Google Earth Pro* measure tool. Two-sample T-Tests assuming unequal variances were conducted in order to determine whether there exist any significant geomorphologic differences between and within groups and sets. Geographic bearings of the ridges were also quantified and T-tests

were completed to determine whether there are any significant differences between or within groups and sets. See Appendix Section 1.

3.2 Ground penetrating radar (GPR) survey

Nineteen approximately strike perpendicular (NW-SE) GPR profiles were acquired along paved roads that cross the entire island (~ 10 km, Fig. 4) using a *MALÅ* push-cart GPR with a 250 MHz antenna. The soil velocity was set to 0.172 m/ns when the GPR was acquired. This method is similar to Moore et al. (2004) who also conducted GPR surveys along a shore-perpendicular road on a sandy barrier island. Two additional profiles of 0.5-1km length were acquired parallel to the strike of the beach ridges in order to get a locally more complete 3-D rendition of the subsurface stratigraphic framework of the ridges.

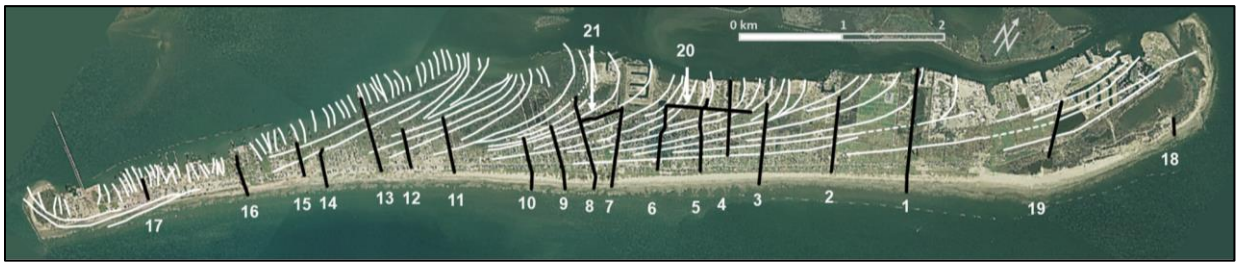

Fig. 4. Beach ridges (white lines) mapped in this study superimposed on modern satellite imagery. GPR profile transects are the numbered black lines.

The data was processed using *GPRSoft* (from Geoscanners). The processing procedures were completed in the following steps: (1) application of a temporal running average filter to remove low frequency signals caused by signal saturation ("de-wowing" the data); (2) application of custom gains to amplify the signal and features at depth; (3) a surface correction to set time zero position to the ground surface; (4) background or noise removal; (5) IIR band pass filter with user-specified frequency boundaries; and (6) migration adaptation to remove unwanted diffractions. These are similar to the processing methods outlined in a review of numerous publications by Neal (2004; Neal & Roberts, 2000).

3.3 Sediment dating and progradation rates

Five sand samples from different beach ridge sets were collected for OSL analysis (Fig. 5) using techniques documented by Lepper (2007) to prevent exposure of the sample to light. The samples were shipped to North Dakota State University's Optical Dating and Dosimetry Lab, where procedures included OSL sample preparation to isolate clean quartz sand, OSL SAR data collection procedures (Murray & Wintle, 2000; Wintle & Murray, 2006; Lepper et al., 2007), OSL equivalent dose distribution analysis (Lepper et al., 2007), and elemental analysis (limited to K, Rb, U, Th) with INAA and dosimetric

analysis (Aitken, 1998; Prescott & Hutton, 1988; 1994; see also Appendix section 4.2). The results were used to determine the age ranges of beach ridge sets and consequently progradation rates and time of formation of Grand Isle.

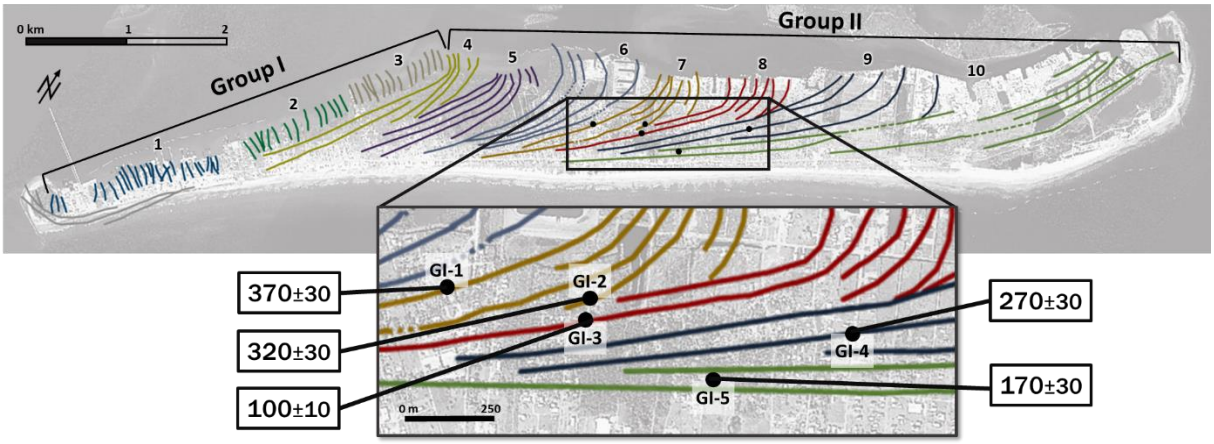

Fig. 5. Location map of six trenches excavated throughout the island to view soil profiles and collect samples for OSL analysis.

Progradation rates were determined by measuring the distance perpendicular to the strike of the ridge set to the shoreline and dividing that by the age difference between the earliest and the latest fully formed ridges. Maximum and minimum rates were determined to account for the uncertainty in the value that arises from uncertainty in the two OSL ages that are involved in each calculation. The mean values are reported in the results section. The statistically derived maximum and minimum ridge accumulation rates were calculated as follows:

Max. ridge accumulation rate (yrs/ridge)

= (max. age older sample – min. age younger sample) = ridge count

Min. ridge accumulation rate (yrs/ridge)

= (min. age older sample – max. age younger sample) = ridge count

At a subsurface depth of 80 cm in the trench dug at sample site GI-3 there was a deposit of shells of unknown origin, primarily *Rangia cuneate* (Gulf wedge clam) and the occasional *Crassostrea virginica* (Atlantic Oyster), forming a layer 10-cm thick. One sample of each species was submitted to Direct AMS Radiocarbon Dating Service for radiocarbon using standard techniques. Results are presented in units of percent modern carbon (pMC) and the uncalibrated radiocarbon age before present (BP). All results were corrected for isotopic fractionation with an unreported $\delta^{13}C$ value measured on the prepared carbon by the accelerator.

3.4 Barrier lithosome volume and sediment transport rate calculations

Conaster (1971) presented isolith maps of two lithosomes below Grand Isle that he mapped using a suite of borings that extended to 80 m depth in the subsurface (Fig. 6). Two lithosomes, designated the "A" sand located within the upper 6 m, and a "B" sand extending from 6 to 20 m in the subsurface were mapped by Conaster (1971). He estimated the "A" sand was deposited no more than 700 yr BP and the underlying "B" sand no more than 1,000 yr BP. These isolith maps collectively provide an opportunity to document the volume of the Grand Isle barrier lithosome. Using these isolith maps of the Grand Isle barrier lithosome ("A" sand) and the sand body at depth ("B" sand), an approximate volume of each was calculated. Each sand body was divided into equally sized squares of a known area and each area was assigned a thickness value derived from the Conaster (1971) isoliths to determine a lithosome volume within each square. Multiple squares were then combined for an estimation of the total volume.

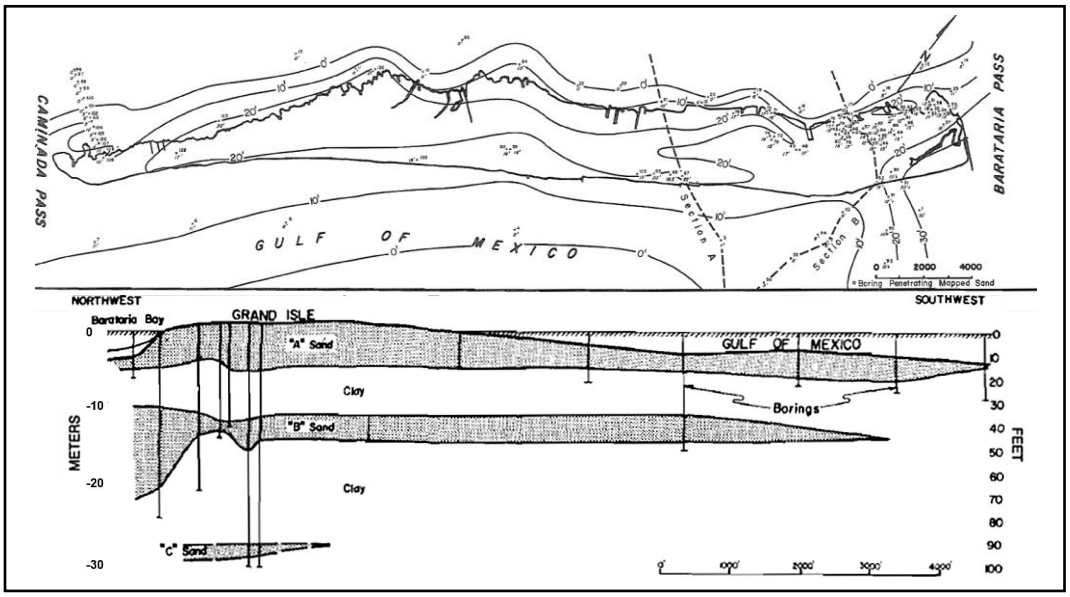

Fig. 6. Conatser (1971) identified two sand bodies which he called the "A" Sand and "B" Sand. Shown here is the isolith map for the "A" Sand. The cross-section (Section B on the isolith map) shows the sand bodies as they exist beneath the eastern end of the island.

Estimates of the sediment fluxes required to establish the "A" sand body were calculated utilizing data from several sources including Caminada Headland erosion rates in McBride et al. (1992), bathymetric change data from List et al. (1994) and Miner et al. (2009), sediment budgets of the Lafourche shoreline calculated by Harper (1977) and Morang et al. (2013), longshore sediment transport rates modelled in Georgiou et al. (2005), and shoreface volumetric change documented in Georgiou et al. (2010). See Appendix Section 4 for details.

3.5 Beach ridge literature review and comparison

Geomorphologic information from 60 sandy, swash-built beach ridge systems from around the world was extracted from 32 studies and compiled for comparison, including: beach ridge width, spacing, and amplitude; age range, width, and number of ridges in the system; average accretion rate and progradation rate. The average accretion rate refers to the number of years needed for one ridge and its associated swale to form, whereas the progradation rate is the rate of outward building measured in meters per year. When one or more of those values were not explicitly stated in the literature, they were calculated from the values that were available. In some studies, the beach ridge systems were divided into individual sets, each with their own characteristic geometric measurements, and these groupings were preserved. In a few instances, where beach ridge plain width was not provided the Google Earth measure tool was used to determine this value. Dune ridges or foredune sequences (Hesp et al., 2005) have not been incorporated, which in some areas are similar in their aspect to beach ridges. See Appendix Section 5 for a summary of the results of this effort.

4. RESULTS

4.1 GPR profiles

Signal penetration in all 21 lines reached a maximum depth of 2-3 m, below which there was signal attenuation or complete absence of coherent reflectors. The two upper-most continuous reflections in all profiles represent air wave and ground wave arrivals respectively and are not part of the stratigraphic data (Neal, 2004). Many of the survey lines were saturated with noise, a term used to describe any measured signal that does not correspond to signals from the desired targets. This is not uncommon in developed settings as nearby objects, buried cables and pipes, and other electromagnetic (EM) emitting equipment are pervasive and all have the capability of creating noise in the profiles (Daniels, 1989; Annan & Daniels, 1998; Olhoeft, 2002; Neal, 2004; Kim et al., 2007). Attenuation of the EM signal by brackish to salty groundwater is common when GPR is conducted on coastal barriers (Jol et al., 1996; van Heteren et al., 1998). Most of the profiles acquired for this study were significantly affected by the presence of salty water at 2-3 m depth, below which the profiles are reflection-free. The depth of the water table was not discernable in most of the profiles. See Appendix Section 2.

The images represent EM energy transmitted through the sediments that is reflected at boundaries between materials with contrasting electrical properties (Daniels, 1989; Davis & Annan, 1989). A reflection can be produced by a change in lithology, grain size, packing, or water saturation (Davis & Annan, 1989). Beach deposit stratification is known to dip either landwards or seawards, but landward dips are less common. The GPR profiles presented here comprise the best examples of both landward- and seaward-dipping reflections (Fig. 7). In figure 7 the line drawings beneath each plot of the digital GPR data are interpretations indicating the prominent reflections. Seaward-dipping reflections are most commonly found in the seaward half of the GPR lines, whereas landward-dipping reflections are mostly observed in the landward half of the GPR lines.

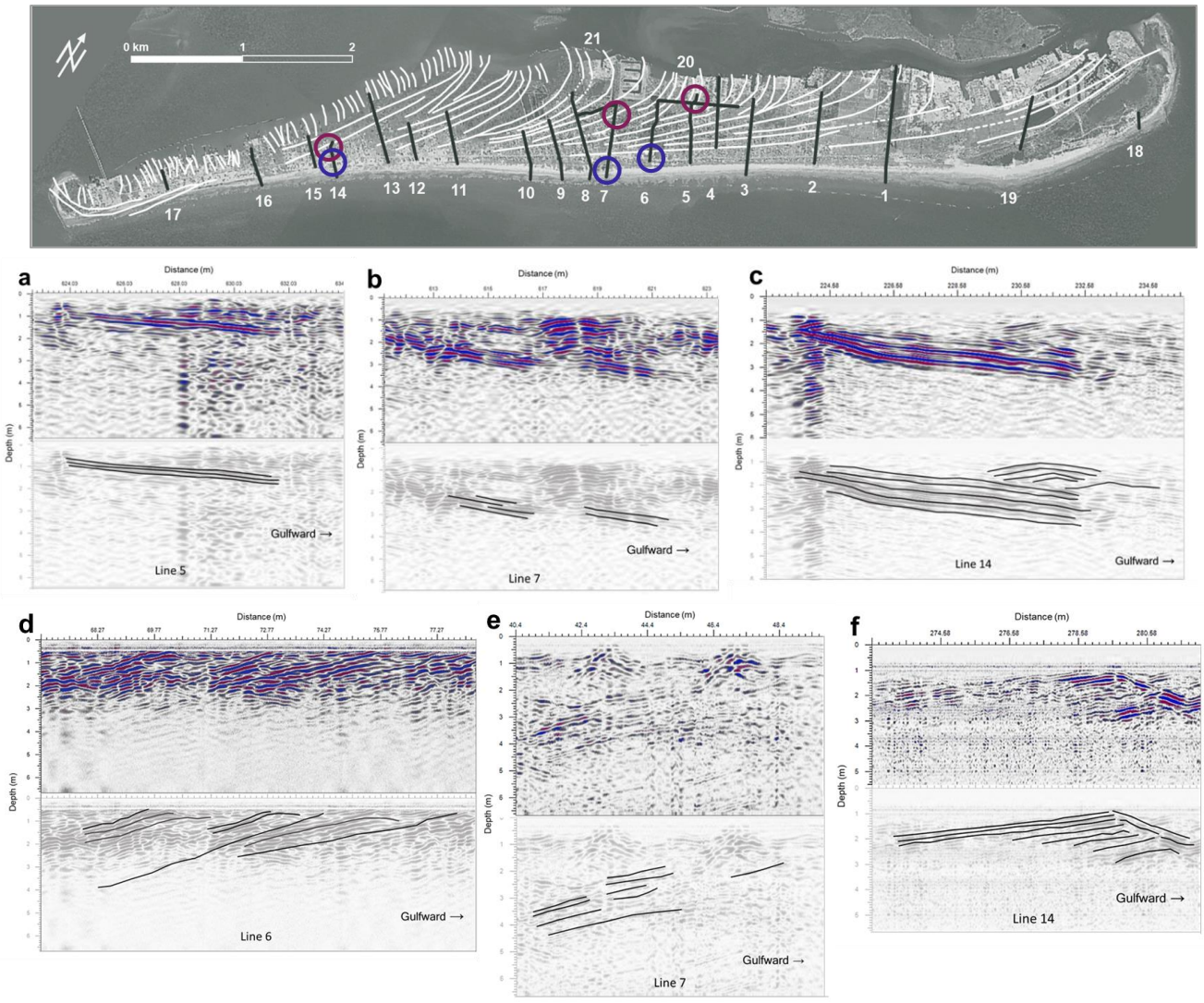

Fig 7. Profiles a through c (red circles on map) are examples of where gulfward-dipping reflections are present and d-f (blue circles on map) are examples of landward-dipping reflections.

Seaward dipping stratification is formed as result of beachface progradation and is usually dissected in places by erosional surfaces resulting from episodic beach retreat. Where the GPR lines extend perpendicular to shore, seaward-, or gulfward-, dipping reflections are prevalent (Fig. 7) as long, mostly continuous, parallel reflections at shallow dip angles. These are interpreted to be signatures of beach progradation, which is expected as the direction of progradation is toward the Gulf of Mexico and would produce Gulfward dipping strata. Daly et al. (2002) and Moore et al. (2004) observed similar signals in profiles acquired perpendicular to the direction of beach progradation.

Landward dipping reflections are also present and tend to exist in one of two locations: (1) toward the back of the island, where the GPR profiles intersect the ridges at oblique angles or (2) paired with a gulfward-dipping reflection. These landward-dipping reflections are representative of beach progradation of the recurved ends of the ridges. Landward-dipping reflections that are found paired with seaward-dipping reflectors are interpreted to represent washover deposits or possibly dunes. Similar results and interpretations are presented in Tamura (2012).

4.2 Planview of ridges

At least 10 distinct sets of beach ridges are present on Grand Isle with the exact number difficult to determine due to the subtlety of their localized separations. Individual sets are separated from one another by truncations causing the older sets to intersect with younger sets at angles that range from approximately 10° to nearly 90°. The sets contain a variable number of individual, subparallel beach ridges with the total number in a set ranging from five to 20. The ridge sets have been divided into two groups (Group I and Group II) based on the pronounced, complete truncation of Group I ridges by those of Group II (Fig. 3).

Group I is comprised of ridge sets 1-3. Only the terminal (lagoonward) ends of these ridges are identifiable in the 1956 imagery and have an average length of 180 m. Spacing between these ridges varies from 31 m to 152 m with an average value of 70 m. The average bearing of these ridge segments is 300° with values ranging from 282° to 327°. For a complete table of ridge spacing and bearing measurements, see Appendix Section 1.

Group II is comprised of ridge sets 4 through 10. The complete ridges of Group II are characterized by longer SW-NE trending sections originating at the gulfward side of the island with either broad or tight westward-curving segments and nearly straight terminal ends that protrude lagoonward. The average length of a complete ridge is approximately 1700 m. Inter-ridge spacing varies from 33 m to 648 m, with an average spacing of approximately 200 m. Inter-ridge spacing at the origins

is generally consistent, whereas spacing at the curves and at termini generally increases from west to east.

The most obvious truncation occurs where Set 4 cuts off sets 1-3, leaving only the tips of these ridges identifiable in the 1956 imagery. There is a significant difference between the average bearings of ridges of Group I and Group II (p-value = 9.34×10^{-8}), reflecting a pronounced change in the direction of progradation from NNE to nearly due east. The angular difference between the progradation directions of the two groups is approximately 20°.

Ridge spacing also differs significantly between Group I and Group II (p-value = 9.8×10^{-8}), thus validating the division of the beach ridges into Groups I and II.

4.3 Sediment dating

In general, the OSL ages decrease in the direction of island growth, which is to be expected due to the overall morphology of the ridges, which indicate east-directed progradation. All but one sample (GI-3) returned ages within the range expected (Table 1). The sample from set 7 (GI-1) was dated at 370±30 yrs, followed by an age of 320±30 yrs for GI-2 from the boundary between ridge sets 7 and 8. Sample G1-4 from set 9 was aged at 270±30 yrs, and sample GI-5 from ridge set 10 was aged at 170±10 yrs. Using the number of ridges between each of these samples as a measure of growth, accretion rates were determined. The length of time required for each set to form only varies by 15 years among the sets (75.5-90.6 yrs). However, sets 1-3 have significantly more ridges, so growth rates were presumably much higher for these sets. See Appendix Section 4 for additional OSL results..

Table 1. OSL age results and related data.

Sample ID	N[1]	M/m[2]	u_t[3]	dD_c[4]	Equivalent Dose[5] (Gy)	Dose Rate[6] (Gy/ka)	Age (yr)	Age Error[7] (yr)	Age Uncert.[8] (yr)
GI1801	95/96	1.01	0.147	1.1%	0.581 ± 0.009	1.579 ± 0.139	370	10	30
GI1802	95/96	1.00	0.126	1.3%	0.547 ± 0.007	1.735 ± 0.148	320	10	30
GI1803	94/96	0.99	0.247	0.6%	0.221 ± 0.006	2.280 ± 0.186	100	10	10
GI1803'	91/96	1.01	0.368	0.6%	0.222 ± 0.009	2.280 ± 0.186	100	10	10
GI1804	95/96	1.01	0.115	0.4%	0.417 ± 0.005	1.572 ± 0.147	270	10	30
GI1805	94/96	0.99	0.185	1.5%	0.258 ± 0.005	1.544 ± 0.120	170	10	10

[1] No. of aliquots used for OSL D_e calculation / no. of aliquots from which OSL data was collected (filtering criteria given in Lepper et al., 2003). [2] Mean/median ratio: a measure of dose distribution symmetry/asymmetry (see supplement to Lepper et al., 2007). [3] Total dose distribution data dispersion (Std. dev./Mean). [4] Dose recovery fidelity (refer to "check dose" in Lepper et al., 2000 and supplement to Lepper et al., 2007). [5] Equivalent doses are based on the mean and std. err. of the OSL D_e distribution. [6] Dose rates calculated following the methods described in Aitken (1985; 1998) and Prescott and Hutton (1988; 1994). [7] Age error based on std. err. of the OSL D_e distribution (Lepper et al., 2011). [8] Fully-propagated age uncertainty (Append. B, Aitken, 1985).

The sample from GI-3 returned an age of 100±10 yrs. Age data sets GI-3 and GI-3' can be considered a test of reproducibility that resulted in consistent ages within the "age error" envelope. This sample (GI-3) is assumed to unknowingly have been collected from disturbed sediment or fill, resulting in the irreconcilable young age. This OSL date was not used in any growth rate calculations. However, there was a deposit of shells of unknown origin at GI-3 at 0.8 m depth. One clam shell and one oyster shell were submitted for radiocarbon dating. The clam sample yielded an age of 1369±24 cal yr BP and the oyster shell was aged at 530±21 cal yr BP. It seems that the *Rangia* shell was washed in and does not represent a true age. The younger date of the oyster shell (530±21 cal yr BP) could represent a maximum age of the sediment layer from which it was extracted. However, the shells were collected from the same sedimentary layer that was OSL dated at 100±10 yrs; therefore, it is likely that neither the OSL nor radiocarbon dates help to confine an age range of the beach ridge from which they were collected.

4.4 Sediment transport rates

The calculated volume of the Grand Isle barrier lithosome ("A" sand) from Conatser's (1971) isolith map is 9.26×10^{-7} m^3. Assuming Grand Isle began forming at approximately 0.75 ka, an average of approximately 123,467 m^3/yr must have been available for deposition during the period of its formation. This relatively large volume of sediment can be reconciled by the high rates of erosion and eastward transport of Caminada beach ridge sand (Table 2, Fig. 8).

Eastern Caminada Headland Erosion Rates		
	Data Source(s)	**Rate (m^3/yr)**
1	Georgiou et al. (2010) + McBride et al. (1992)	334,740
2	Harper (1977)	305,950
3	Miner et al. (2009) + McBride et al. (1992)	309,176
4	List et al. (1994) + McBride et al. (1992)	291,023
5	Morang et al. (2013)	191,000*
6	Georgiou et al. (2005)	146,000*
	Mean:	262,982

* Excludes fine-grained sediment

Table 2. Estimates of Caminada Headland erosion rates were calculated from several sources or combinations of sources.

The volume of the "B" sand is approximately 1.6×10^9 m^3, nearly two orders of magnitude larger than that of the Grand Isle barrier lithosome. Using Conatser's (1971) estimated age of the base of the "B" sand bed at about 0.97 ka and our estimate here of Grand Isle's oldest beach ridges forming about 0.72 ka, we estimate that it took approximately 0.25 kyr for the "B" sand and the prodelta clays that lie above it to be deposited. A general rate at which the "B" sand was deposited can be determined by dividing its calculated volume of 1.6×10^9 m^3 by 0.25 ka for a depositional rate of approximately 5×10^6 m^3/yr.

4.5 Grand Isle growth rates

Progradation rates, or seaward/longshore extension of the island, calculated for sets 4-10 range from 9.1 m/yr to 27.0 m/yr with an average rate of 14.9 m/yr. Accretion rates, or the number of years required for one ridge to form, ranged from 12.9 to 15.1 yr/ridge with an average of approximately 14.8 yr/ridge.

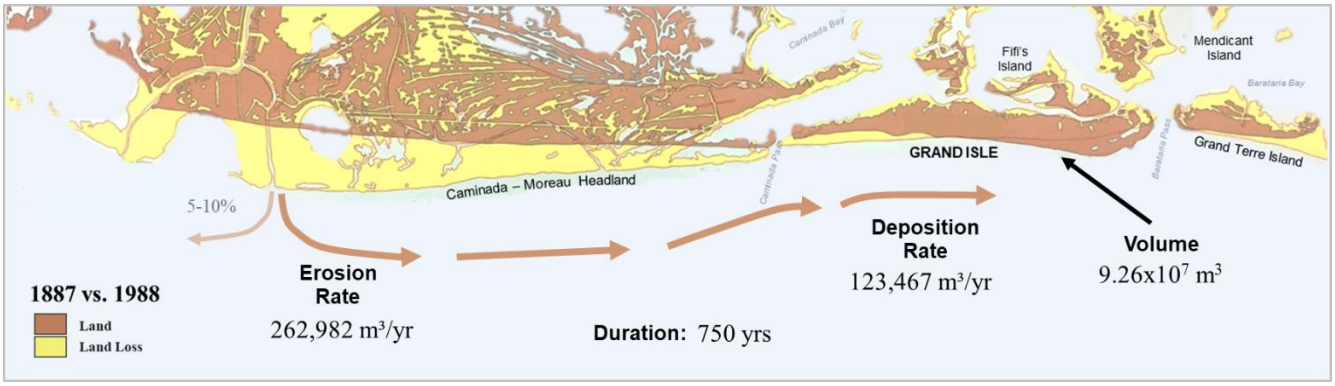

Fig 8. Map showing the Caminada Headland was eroding at more than twice the rate needed to supply Grand Isle's growth (modified from McBride et al., 1992).

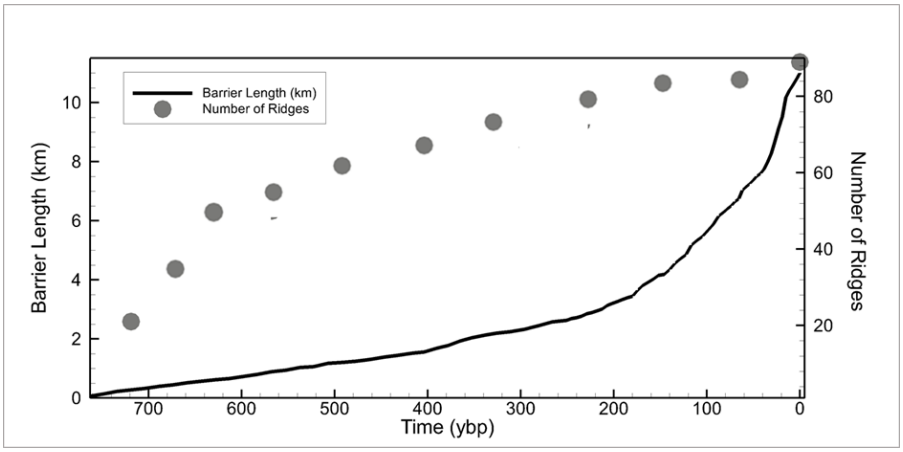

Fig. 9. Barrier length (progradation) versus number of ridges (accretion) comprising the Grand Isle beach ridge plain over time. Note that when the progradation rate is highest (~0-50 ybp), accretion rate is lowest. This is manifested as wider, more spaced out ridges, possibly due to decreasing accommodation space.

Figure 9 is a plot of the progradation of Grand Isle along the island's long axis through time. A steady, slow rate of increase persisted for approximately 0.5 kyr, at which time the growth rate increased until present day. In the past 0.2 kyr (30% of total growth time), the island has increased in length by 8000 m (72% of total length). See Section 4 of the Appendix for growth rate calculations.

The figure also illustrates the relationship between time and growth of the beach ridge plain. It makes clear that the rate of ridge accumulation in the first ~200 years was markedly higher than that of the past ~0.5 kyr. This corresponds to the relatively close, uniform ridge spacing of Group I ridges and those of Group II that exhibit increasing spacing in a westward direction.

4.6 Beach ridge plain comparisons

Of the 60 global beach ridge sets examined through a literature review, 39 formed during a relative sea level rise, including Grand Isle. Despite the similarities in depositional setting (barrier), sea level trend (rising) and proximity of the northwestern Florida barrier sets studied, Grand Isle had significantly higher growth rates than the other beach ridge systems. This could be accounted for by the presence of substantially different sediment sources; Grand Isle is sourced by a continuously and rapidly eroding adjacent beach ridge plain. Barriers in Florida for example are typically derived from multiple sources, sediment from the shelf, alongshore sources, and existing barrier islands (Stapor et al., 1991; Stone et al., 1992). Sediment was supplied in pulses with minor sea level fluctuations that resulted in an initial depositional phase followed by an erosional phase as the supply rate fell below a critical threshold (Stapor et al., 1991).

The average progradation rate calculated for both Group I ridges (18.43 m/yr) and Group II ridges (14.61 m/yr) of Grand Isle are more than four times the average rate for all other examined beach ridge plains (3.25 m/yr) (Fig. 9). Grand Isle's progradation rates are wholly isolated at the top of the range; the closest set is the Sacalin beach ridge set of the Danube River delta area (13.33 m/yr; Vespremeanu et al., 2016). Similar to the Grand Isle beach ridge plain, the Sacalin is a delta- headland flanking barrier spit.

The average accretion rate, or the length of time required for one ridge to form, calculated for Group I ridges of Grand Isle (0.21 ridges/yr) is more than double the average rate for all other examined beach ridge plains (0.051 ridges/yr). The accretion rate for Group II is only slightly higher at 0.06 ridges/yr. As with progradation rates, it is the beach ridge plains of the Danube system (Vespremeanu et al., 2016) that have accretion rates closest to those of Grand Isle (Sacalin- 0.167 ridges/yr; Buhaz- 0.086 ridges/yr; New Peritеasca- 0.08 ridges/yr).

A clear relationship is present between progradation rate and accretion rate for all BRPs studied: as accretion rate (ridges/yr) increases, progradation rate (m/yr) increases (Fig. 10). Therefore, if ridges are forming quickly (<50 yr/ridge), then the seaward progradation of the barrier is generally rapid.

The earlier ridge set growth was initiated, the larger the range of accretion rates. For BRPs older than 1 kyr, accretion rates vary from 0.311 ridges/yr to 0.003 ridges/yr. Younger beach ridge sets (< 1 kyr) formed ridges at a uniformly rapid pace, most requiring < 50 yr/ridge. The range of accretion rates increases with increasing age of BRP initiation.

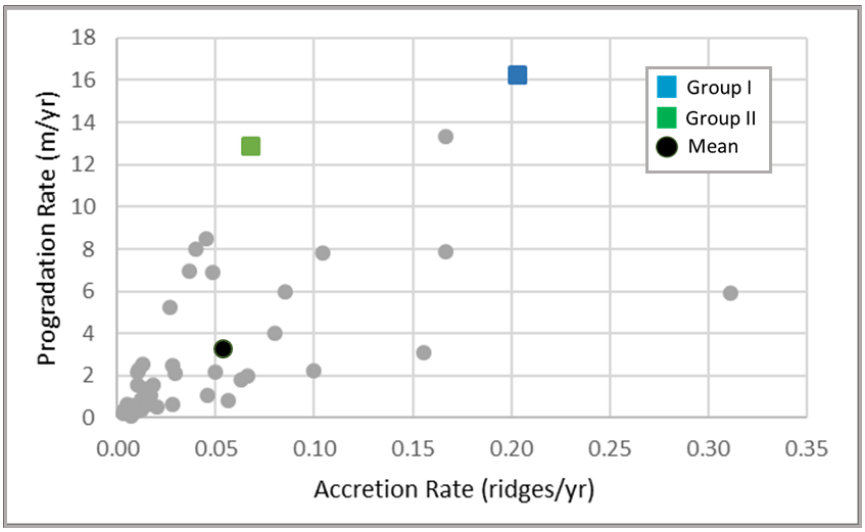

Fig. 10. Estimates of Caminada Headland erosion rates were calculated from several sources or combinations of sources.

For BRPs that formed in 0.6 kyr or less (about half of those examined), progradation rates vary widely from about 1 m/yr to 19 m/yr. For those BRPs that took longer than 0.6 kyr to form, none exceeded a progradation rate of 3 m/yr. Progradation rates were slower for BRPs that took longer to form.

5. DISCUSSION

Growth rates of beach ridges are well documented (Davies, 1958; Carter, 1986) and are highly variable. Generally, high rates of sediment influx are reflected in smaller ridge dimensions, whereas large beach ridges indicate periods of reduced sediment availability (Johnson, 1919; Davies, 1958; Psuty, 1966). Davies (1958) emphasized that rapid deposition resulted in low and closely spaced ridges with very regular profiles, whereas slower deposition resulted in characteristically longer ridges with wider swales and an irregular profile. The Group II ridges of Grand Isle exhibit both characteristics, beginning as more closely spaced ridges at the western end evolving into more irregularly and widely spaced ridges towards the east.

The landward edge of Grand Isle reflects the geomorphic imprint of the recurved spit process described by Otvos (2000). Recurved ridges, at places, support lagoonward prominences of the shoreline. The inter-ridges are marked by lagoonal reentrants, and along with the ridges, they markedly

influence the crenulate outline of the lagoonal shoreline (Conatser, 1971). Many of the shore-perpendicular fingerlike projections separated by elongated lagoonal reentrants are identified in figure 3.

For some period of time before 0.57 ka, Group I ridges began prograding at a rapid pace as the shoreface of the newly formed Caminada beach ridge plain eroded, providing a steady supply of sand to form the closely spaced ridges. The main shafts, or Gulfward portions, of the beach ridges would have extended approximately 2 km farther into the Gulf of Mexico, along strike of the Caminada headland at that time (Fig. 11).

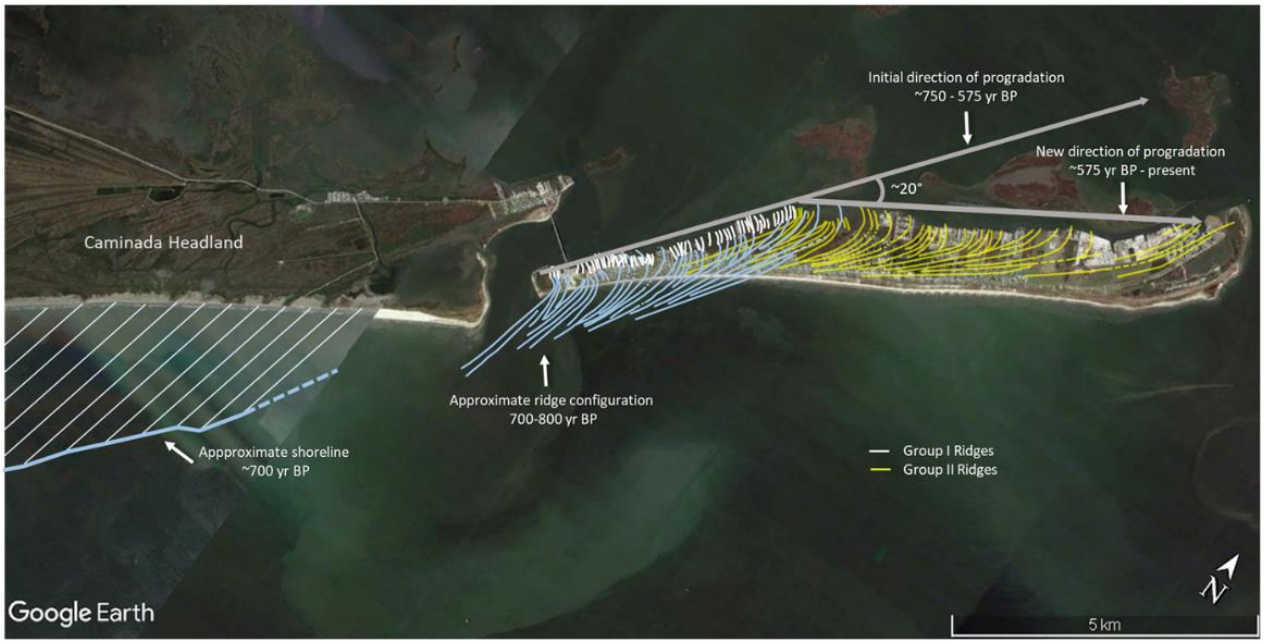

Fig. 11. Schematic of approximate eastern Barataria coastal configuration approximately 0.7 ka. The orientation of Group I ridges and the former position of the Caminada headland shoreline reveal a striking alignment that strongly suggests that erosion rates and change in shoreline configuration of the Caminada headland kept pace with the accretion and directional progradation change of the beach ridges of Grand Isle.

At approximately 0.57 ka, the ridges of Group II began to accrete. The major truncation of Group I ridges by Group II (Fig. 3) seems to indicate a period of decreased sediment supply and erosion of a large portion of those ridges. Subsequently, the sediment supply returned and progradation resumed albeit in a direction that was different by approximately 20°. This resulted in the tips of Group I ridges intersecting the younger ridges of Group II at nearly a 90° angles. Sets 5-8 grew at relatively stable rates with moderately even spacing. Sets 9 and 10, however, become increasingly spaced out. Assuming that sediment supply, wave climate, and storm frequency remained the same, a factor that could account for the change in spacing through time is a decrease in accommodation space toward the east. Historical bathymetry as far back as the 1870's (List et al., 1994; 1997) and a historical map from the 1700s (Gauld, 1771) indicate that the present-day northeastern end of Grand Isle had shallower nearshore depths than

the southwestern end. As Grand Isle prograded in a northeastern direction the sediment had less vertical space to fill and therefore spread out laterally. These shallower nearshore depths at the eastern end of the island are a result of ebb tidal delta formation at Barataria Pass (FitzGerald et al., 2004).

The body of sand underlying Grand Isle (Conatser's "B" sand) was transported west by the westerly littoral currents that existed prior to the outbuilding of the modern "birdfoot" delta complex into the Gulf of Mexico beginning around 350 yr BP (Penland et al., 1986; Gerdes, 1982; Frazier, 1967; Kolb & Van Lopik, 1958). Following abandonment, the distributary mouth bars and beach ridges of Bayou Blue and the Plaquemines subdelta were transformed into numerous small erosional headland sand sources. These sediments were transported west and formed the sandy platform (Conatser's "B" sand) upon which Grand Island eventually was deposited. It likely was also the major source for construction of the Caminada beach ridge complex, which would, in turn, become the source for building Grand Isle.

When eustatic sea level rise slowed, initial lobes from the St. Bernard complex prograded into the area and fine-grained interlobe basin fill sediments were deposited. Relative sea level became stabilized at approximately 3 ka (Coleman & Smith, 1964). The initial St. Bernard lobes started to

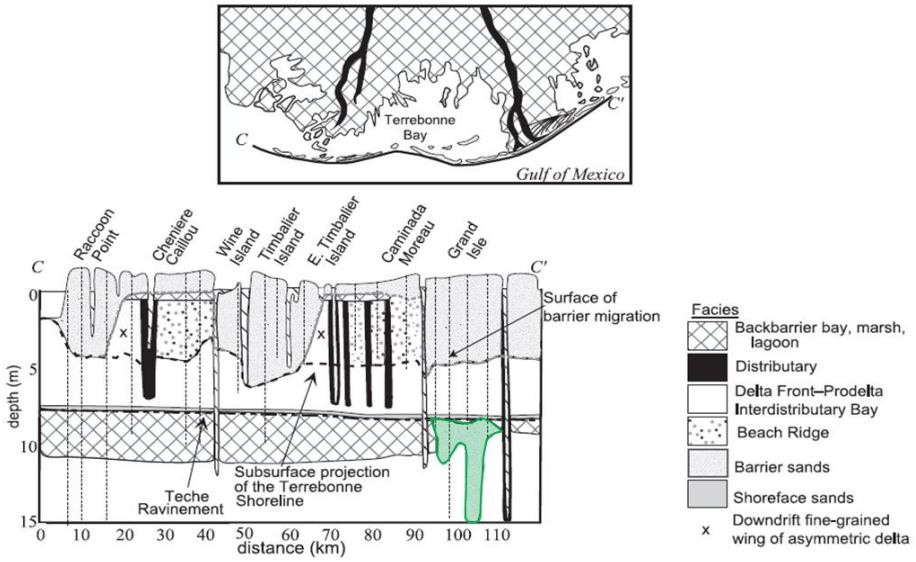

Fig. 12. Shore-parallel cross section extending from the Caillou Bay to Caminada–Moreau headland. The "B" sand that Conatser (1971) identified is present (*green*) and may contribute to the stability of Grand Isle (modified from Kulp, et al. (2005) based on data from Penland et al. (1988), and cores and cross sections presented by May et al. (1984), Neese (1984), Gerdes (1982), Isacks (1983), SJB Group (2003), and unpublished Louisiana Geological Survey data).

become abandoned and their distributary sands were reworked into the Teche shoreline (Penland et al. 1986), of which Bayou des Families was part. Figure 12 from Kulp et al. (2005) identifies the Teche ravinement in cross section at about 8-10 m depth along the coast from just west of Terrebone Bay to just east of Barataria Pass. The ravinement truncates backbarrier bay, marsh, and lagoon deposits in the west along Terrebone bay, but barrier sands underlie the prodelta deposits in the east beneath Grand Isle. The presence of this sand body at depth found exclusively beneath Grand Isle could be one of

several stabilizing factors for the island. Deltaic sediment has the potential to consolidate significantly under load due to reduction in void space and decay of organic matter (Kuecher, 1994). However, beneath Grand Isle, this deltaic sediment is absent at 8-10 m depth and present instead is less compactible barrier sand.

The values in Table 2 of the text represent a range of possible rates of sediment transport from the eastern Caminada headland to Grand Isle. All but one rate, reported by Georgiou et al. (2005), indicate that more than enough sediment is transported northeastward from the headland to Grand Isle in order for the island to have been formed in 0.8 kyr, or even as little as 0.6 kyr. This means the island may indeed be younger than previously thought as sediment supply appears to not have been a limiting factor for island growth.

The rates of erosion and transport are assumed to be linear here, although this is likely not the case. It is more likely that rates of erosion of the Caminada headland were much higher in the earlier stages than they have been in recent times because (1) the shoreline would have been more irregular and therefore more susceptible to coastal straightening, and (2) the shoreface would have been steeper to approaching waves resulting in more erosion (Miner et al., 2009).

Comparing the reconstruction of the Caminada headland shoreline position approximately 0.7 ka with that of the projected Group I beach ridges around the same time (Fig. 11) reveals a striking alignment that strongly suggests that erosion rates and change in shoreline configuration of the Caminada headland kept pace with the accretion and directional progradation change of the beach ridges of Grand Isle. When rates of shoreline change of the Caminada headland provided by McBride et al. (1992) are extended further back in time to about 0.7 ka, it is clear that the distance in the Gulf to which the headland protrudes relative to the present shoreline increases from east to west.

6. CONCLUSIONS

With the identification and analysis of 90 new beach ridges some observations first made by Conatser (1971) are substantially refined regarding the geomorphology and history of Grand Isle's formation.

The erosion and transport rates of the Caminada headland sediment were more than sufficient for the development of the Grand Isle barrier lithosome in the estimated time frame of approximately the last 750 years. Although the rate of erosion of the Caminada headland has likely decreased through

time as the headland became straighter and reoriented oblique to the incoming wave direction, sediment supply remains high enough to facilitate the growth of Grand Isle.

OSL dating provided a reliable method for establishing beach ridge growth rates for Group II ridges. However, for the older Group I ridge segments, which are difficult to locally impossible to access because of current island infrastructure, approximate growth rates for this part of the island were determined in another fashion. The primary approach of quantifying growth rates for these ridge sets was to use ridge spacing, volumetric calculations, and sediment transport rates derived from dates obtained for Group I to establish approximately when Grand Isle Group I beach ridges began forming. On the basis of this approach an estimated age of 0.75 kyr, is presented herein for the initiation of island growth, which closely aligns with the age of 0.7 kyr proposed by Conatser (1971).

Previous studies have estimated the remaining life of Grand Isle only using past rates of shoreline change (e.g. McBride & Byrnes, 1997; Penland & Suter, 1988; Harper, 1977) but should be updated to include parameters investigated in this study, including subsurface stratigraphy. Considering the relatively high rate of sediment supply, the large volume of the Grand Isle lithosome, and the presence of the underlying preexisting sand body ("B" sand), the island lifespan may extend even further into the future than the 950-yr lifespan estimated by McBride et al. (1995).

Assuming the incident wave direction and sediment supply have been approximately constant during the past 0.5 kyr, the most likely cause for the decreasing westward density of Group II ridges is reduced accommodation that existed as the island prograded east. Although not evaluated fully in this study, some combination of change in the rate of relative sea-level rise and a change in wave energy and direction may be responsible for the truncation between, and the different orientations, of Group I and Group II ridges. Additional insight into these relationships and the underlying cause may be possible with the collection of additional ridge ages as well as stratigraphic relationships provided by additional GPR surveys and coring.

There were also difficulties with the collection and subsequent analysis of GPR data that was collected on Grand Isle. The dense development on the island meant above- and below-ground utilities contaminated the data with ringing, rendering entire lines of data unusable. Additionally, the inability to take cores in the substrate of dry, packed sand prevented the ability to verify subsurface lithostratigraphy that was imaged in the GPR reflections.

OSL dating is a suitable method for dating the timing of deposition of quartz-rich sands on this section of the Gulf of Mexico coast, and further use of OSL dating to enhance our understanding of Holocene coastal evolution in the region should be pursued. The development of such a chronology

enables a spatiotemporal reconstruction of the coastline at the local scale, and therefore an understanding of geomorphological responses to Holocene relative sea level changes, allowing accurate predictions of future responses in the face of climate change. Relative to a global sample of sandy beach ridge plains, Grand Isle both prograded and accreted at faster rates. However, as sea level rises, it will likely become difficult to maintain these progradation rates without an additional sediment supply.

In the face of historically high rates of relative sea level rise across the Mississippi River delta plain (Penland & Ramsey, 1990; Dubois, 2002; Georgiou et al., 2005; FitzGerald et al., 2006), shoreline retreat, and bathymetric change (Miner et al., 2009), this information can aid managers in decision-making for future mitigation efforts along the Louisiana coast (CPRA, 2017).

WORKS CITED

Aitken, M. J. (1985). *Thermoluminescence dating*. London: Academic Press.

Aitken, M. J. (1998). *An introduction to optical dating*. New York, NY: Oxford University Press.

Ballarini, M., Wallinga, J., Murray, A. S., Van Heteren, S., Oost, A. P., Bos, A. J. J., & Van Eijk, C. W. E. (2003). Optical dating of young coastal dunes on a decadal time scale. *Quaternary Science Reviews, 22*(10), 1011-1017. https://doi.org/10.1016/S0277-3791(03)00043-X

Batten, B. K., Ebersole, B. A., King, D. B., Smith, E. R. (2004) Coastal Processes Assessment and Project Re-Evaluation: Grand Isle, Louisiana, Shore Protection Project (DRAFT). U.S. Army Corps of Engineers Engineer Research and Development Center, ERDC/CHL TR-04.

Belperio, A. P. (1983). Terrigenous sedimentation in the central Great Barrier Reef lagoon: a model from the Burdekin region. *BMR Journal of Australian Geology and Geophysics*, *8*(3), 179-190.

Bowman, G., & Harvey, N. (1986). Geomorphic evolution of a Holocene beach-ridge complex, LeFevre Peninsula, South Australia. *Journal of Coastal Research*, 345-362.

Brill, D., Jankaew, K., & Brückner, H. (2015). Holocene evolution of Phra Thong's beach-ridge plain (Thailand)—chronology, processes and driving factors. *Geomorphology*, *245*, 117-134. https://doi.org/10.1016/j.geomorph.2015.05.035

Bristow, C. S., & Pucillo, K. (2006). Quantifying rates of coastal progradation from sediment volume using GPR and OSL: the Holocene fill of Guichen Bay, south-east South Australia. *Sedimentology, 53*(4), 769-788. https://doi.org/10.1111/j.1365-3091.2006.00792.x

Brooke, B., Lee, R., Cox, M., Olley, J., & Pietsch, T. (2008a). Rates of shoreline progradation during the last 1700 years at Beachmere, Southeastern Queensland, Australia, based on optically stimulated luminescence dating of beach ridges. *Journal of Coastal Research,* 640-648. https://doi.org/10.2112/04-0375.1

Brooke, B., Ryan, D., Pietsch, T., Olley, J., Douglas, G., Packett, R., ... & Flood, P. (2008b). Influence of climate fluctuations and changes in catchment land use on Late Holocene and modern beach-ridge sedimentation on a tropical macrotidal coast: Keppel Bay, Queensland, Australia. Marine Geology, 251(3-4), 195-208.

Carter, R. W. G. (1986). The morphodynamics of beach-ridge formation: Magilligan, Northern Ireland. *Marine Geology, 73*(3-4), 191-214. https://doi.org/10.1016/0025-3227(86)90015-0

Church, J. A. & White, N. J. (2011). Sea-level rise from the late 19th to the early 21st century. *Surveys in geophysics*, *32*(4-5), pp.585-602.Coastal Protection and Restoration Authority of Louisiana (CPRA). 2017. Louisiana's Comprehensive Master Plan for a Sustainable Coast. Coastal Protection and Restoration Authority of Louisiana. Baton Rouge, LA.

Clemmensen, L. B., Nielsen, L., Bendixen, M., & Murray, A. (2012). Morphology and sedimentary architecture of a beach-ridge system (Anholt, the Kattegat sea): a record of punctuated coastal progradation and sea-level change over the past~ 1000 years. *Boreas*, *41*(3), 422-434. https://doi.org/10.1111/j.1502-3885.2012.00250.x

Coleman, J. M., & Smith, W. G. (1964). Late Recent rise of sea level. *Geological Society of America Bulletin*, *75*(9), 833-840. https://doi.org/10.1130/0016-7606(1964)75[833:LRROSL]2.0.CO;2

Combe, A. J., & Soileau, C. W. (1987). Behavior of man-made beach and dune, Grand Isle, Louisiana. In Coastal sediments (pp. 1232-1242). ASCE.

Conatser, W. E. (1971). Grand Isle: a barrier island in the Gulf of Mexico. *Geological Society of America Bulletin, 82*(11), 3049-3068. https://doi.org/10.1130/0016-7606(1971)82[3049:GIABII]2.0.CO;2

Curray, J. R., Emmel, F. J., & Crampton, P. J. (1969). Holocene history of a strand plain, lagoonal coast, Nayarit, Mexico. In *Memorias del Simposio Internacional de Lagunas Costeras* (pp. 63-100).

Daniels, J. J. (1989, March). Fundamentals of ground penetrating radar. In *Proceedings of the Symposium on the Application of Geophysics to Engineering and Environmental Problems* (pp. 62-142). Colorado School of Mines, Golden, CO. https://doi.org/10.4133/1.2921864

Davies, J. L. (1958). Analysis of Height Variation in Sand Beach-ridges. *Australian Journal of Science, 21*, 51-52.

Davis, J. L., & Annan, A. P. (1989). Ground-penetrating radar for high-resolution mapping of soil and rock stratigraphy. *Geophysical prospecting*, *37*(5), 531-551.

DePratter, C. B., & Howard, J. D. (1977). History of shoreline changes determined by archaeological dating: Georgia coast, USA. *Gulf Coast Association of Geological Societies Transactions, 27*, 252-258.

Dokka, R. K. (2006). Modern-day tectonic subsidence in coastal Louisiana. *Geology*, *34*(4), pp.281-284.

Dokka, R. K., Sella, G. F., & Dixon, T. H. (2006). Tectonic control of subsidence and southward displacement of southeast Louisiana with respect to stable North America. *Geophysical Research Letters*, *33*(23). doi:10.1029/ 2006GL027250

Doyle, T. W. (2009). Hurricane frequency and landfall distribution for coastal wetlands of the Gulf coast, USA. *Wetlands*, *29*(1), 35-43.

Dubois, R.N. (2002). How does a barrier shoreface respond to a sea-level rise?. *Journal of Coastal Research*, *18*(2).

Edrington, C. H., Blum, M. D., Nunn, J. A. & Hanor, J. S. (2008). Long-term subsidence and compaction rates: A new model for the Michoud area, south Louisiana. *Transactions of the Gulf Coast Assoc. Geol. Soc*., 58, 261–272.

Engels, S., & Roberts, M. C. (2005). The architecture of prograding sandy-gravel beach ridges formed during the last Holocene highstand: Southwestern British Columbia, Canada. *Journal of Sedimentary Research*, *75*(6), 1052-1064. https://doi.org/10.2110/jsr.2005.081

Fitzgerald, D. M., Baldwin, C. T., Ibrahim, N. A., & Humphries, S. M. (1992). Sedimentologic and morphologic evolution of a beach ridge barrier along an indented coast: Buzzards Bay, Massachusetts. In *Quaternary Coasts of the United States: Marine and Lacustrine Systems*, Fletcher III, C. H. & Wehmiller, J. F. (Eds.). SEPM Special Publication No. 48, 65-75.

Fitzgerald, D. M., Cleary, W. J., Buynevich, I. V., Hein, C. J., Klein, A., Asp, N., & Angulo, R. (2007). Strandplain evolution along the southern coast of Santa Catarina, Brazil. *Journal of Coastal Research,* 152-156. 152-156. https://www.jstor.org/stable/26481574

Fitzgerald, D. M., Kulp, M., Penland, S., Flocks, J. & Kindinger, J. (2004). Morphologic and stratigraphic evolution of muddy ebb-tidal deltas along a subsiding coast: Barataria Bay, Mississippi River delta. *Sedimentology*, *51*(6), pp.1157-1178. https://doi.org/10.1111/j.1365-3091.2004.00663.x

Frazier, D.E. (1967). Recent deltaic deposits of the Mississippi Rivet their development and chronology. *Gulf Coast Association of Geological Societies Transactions, 17*, 287-315.

Gauld, G. (1777). "An Accurate Chart of the Coast of West Florida, and the Coast of Louisiana…". Published 1823, London.

Georgiou, I. Y., FitzGerald, D. M., & Stone, G. W. (2005). The impact of physical processes along the Louisiana coast. *Journal of Coastal Research*, 72-89. https://www.jstor.org/stable/25737050

Georgiou, I. Y., & Schindler, J. K. (2009). Wave forecasting and longshore sediment transport gradients along a transgressive barrier island: Chandeleur Islands, Louisiana. *Geo-Marine Letters*, *29*(6), 467-476.

Georgiou, I., Weathers, H. D., Kulp, M. A., Miner, M. & Reed, D. J. (2010). Interpretation of Regional Sediment Transport Pathways using Subsurface Geologic Data. Draft Final Report submitted to US Army Corps of Engineers, CESU Contract # W912HX-09-2-0027.

Gerdes, R. G. (1982). Stratigraphy and history of the development of the Caminada-Moreau beach ridge plain, southeast Louisiana: Unpublished M.S. thesis, Louisiana State University, Baton Rouge, 185 p.

Goy, J. L., Zazo, C., & Dabrio, C. J. (2003). A beach-ridge progradation complex reflecting periodical sea-level and climate variability during the Holocene (Gulf of Almeria, Western Mediterranean). *Geomorphology*, *50*(1-3), 251-268. https://doi.org/10.1016/S0169-555X(02)00217-9

Grzegorzewski, A., & Georgiou, I. Y. (2011). Sediment transport trends along an island terminus: A model study during storms at the northern Chandeleur Islands. In *The Proceedings of the Coastal Sediments 2011: In 3 Volumes* (pp. 2198-2211). https://doi.org/10.1142/9789814355537_0165

Harper, J. (1977). Sediment dispersal trends of the Caminada-Moreau beach-ridge system. *Gulf Coast Association of Geological Societies Transactions, 27*, 283-289.

Hede, M. U., Sander, L., Clemmensen, L. B., Kroon, A., Pejrup, M., & Nielsen, L. (2015). Changes in Holocene relative sea-level and coastal morphology: A study of a raised beach ridge system on Samsø, southwest Scandinavia. *The Holocene*, *25*(9), 1402-1414. https://doi.org/10.1177/0959683615585834

Hein, C. J., FitzGerald, D. M., Cleary, W. J., Albernaz, M. B., Menezes, D., Thadeu, J., & Klein, A. H. D. F. (2013). Evidence for a transgressive barrier within a regressive strandplain system: Implications for complex coastal response to environmental change. *Sedimentology*, *60*(2), 469-502. https://doi.org/10.1111/j.1365-3091.2012.01348.x

Hesp, P. A. (1984). The formation of sand "beach ridges" and foredunes. *Search*, *15*(9-10), 289-291.

Hesp, P. A., Dillenburg, S. R., Barboza, E. G., Tomazelli, L. J., Ayup-Zouain, R. N., Esteves, L. S., ... & Clerot, L. C. (2005). Beach ridges, foredunes or transgressive dunefields? Definitions and an examination of the Torres to Tramandaí barrier system, Southern Brazil. *Anais da Academia Brasileira de Ciências*, *77*(3), 493-508. http://dx.doi.org/10.1590/S0001-37652005000300010

Ivins, E. R., Dokka, K., & Blom, R. (2007). Post-glacial sediment load and subsidence in coastal Louisiana. *Geophysical Research Letters, 34*, L16303. doi:10.1029/2007GL030003

Jafari, N. H., Harris, B. D., & Stark, T. D. (2018). Geotechnical investigations at the Caminada Headlands beach and dune in coastal Louisiana. *Coastal Engineering*, *142*, 82-94. https://doi.org/10.1016/j.coastaleng.2018.04.014

Johnson, D. W. (1919). *Shore processes and shoreline development*. John Wiley & Sons, Incorporated.

Johnson, R., Glaccum, R., & Wojtasinski, R. (1979). Application of ground penetrating radar to soil survey. Soil survey. In *Soil and Crop Science Society of Florida Proceedings* (Vol. 39, pp. 2-4). doi:10.2136/sh1982.3.0017.

Jol, H. M., Smith, D. G., & Meyers, R. A. (1996). Digital ground penetrating radar (GPR): a new geophysical tool for coastal barrier research (Examples from the Atlantic, Gulf and Pacific Coasts, USA). *Journal of Coastal Research*, 960-968. https://www.jstor.org/stable/4298546

Jurkowski, G., Ni, J., & Brown, L. (1984). Modern uparching of the Gulf coastal plain. *Journal of Geophysical Research, 89*, 6247-6262.

Kazmann, R. G. & Heath, M. M. (1968). Land subsidence related to ground-water offtake in the New Orleans area. *Transactions Gulf Coast Association of Geological Societies, 18,* 108–113.

Kim, J. H., Cho, S. J., & Yi, M. J. (2007). Removal of ringing noise in GPR data by signal processing. *Geosciences Journal*, *11*(1), 75-81.

Kolb C. R. & Van Lopik, J. R. (1958). Geology of the Mississippi River Deltaic Plain, Southeastern Louisiana: United States Army Corps of Engineers, Waterways Experiment Station, Technical Reports 3-483 and 3-484, Vicksburg, MS.

Krinsley, D. H., & Donahue, J. (1968). Environmental interpretation of sand grain surface textures by electron microscopy. *Geological Society of America Bulletin, 79*(6), 743-748. https://doi.org/10.1130/0016-7606(1968)79[743:EIOSGS]2.0.CO;2

Kuecher, G. J. (1994). "Geologic Framework and Consolidation Settlement Potential of the Lafourche Delta, Topstratum Valley Fill; Implications for Wetland Loss in Terrebonne and Lafourche Parishes, Louisiana." *LSU Historical Dissertations and Theses*. Available at 5734. https://digitalcommons.lsu.edu/gradschool_disstheses/5734

Kulp, M., Fitzgerald, D., & Penland, S. (2005). Sand-rich lithosomes of the Holocene Mississippi River delta plain, *in River Deltas-Concepts, Models, and Examples, Spec. Publ. SEPM Society for Sedimentary Geology, 83*, 279–293. https://doi.org/10.1130/G23665A.1

Leatherman, S. P., Rampino, M. R., & Sanders, J. E. (1983). Barrier island evolution in response to sea level rise; discussion and reply. *Journal of Sedimentary Research, 53*(3), 1026-1033. https://doi.org/10.1306/212F8314-2B24-11D7-8648000102C1865D

Lepper, K., Agersnap-Larsen, N., & McKeever, S.W.S. (2000). Equivalent dose distribution analysis of Holocene aeolian and fluvial quartz sands from Central Oklahoma. *Radiation Measurements, 32*, 603–608.

Lepper, K., Wilson, C., Gardner, J., Reneau, S. and Levine, A. (2003) Comparison of SAR techniques for luminescence dating of sediments derived from volcanic tuff. *Quaternary Science Reviews, 22*, 1131-1138.

Lepper, K., Fisher, T. G., Hajdas, I., & Lowell, T. V. (2007i*Geology, 35,* 667–670.

Lepper, K., Gorz, K., Fisher, T. G., & Lowell, T. (2011). Age determinations for glacial Lake Agassiz shorelines west of Fargo, North Dakota, U.S.A. *Canadian Journal of Earth Sciences, 48,* 1199–1207.

Lepper, K., Argyilan, E., & Fisher T. (2017). Pushing the limits of OSL application to Great Lakes costal deposits: How young and how small? *GSA Abstracts with Programs, 49*(2). doi: 10.1130/abs/2017NE-291582.

List, J. H., Jaffe, B. E., Sallenger Jr, A. H., Williams, S. J., McBride, R. A., & Penland, S. (1994). *Louisiana barrier island erosion study; atlas of sea-floor changes from 1878 to 1989*(No. 2150-B).

List, J. H., Jaffe, B. E., Sallenger Jr, A. H. and Hansen, M. E. (1997). Bathymetric comparisons adjacent to the Louisiana barrier islands: Processes of large-scale change. *Journal of Coastal Research*, pp.670-678. https://www.jstor.org/stable/4298662

Louisiana Department of Natural Resources (LDNR) (2007). Grand Isle Barrier Shoreline Stabilization Study, Preliminary Engineering Report, Part 1: Basis of Engineering. DNR Contract No. 2512-05-05.

Martinez, L., O'Brien, S., Bethel, M., Penland, S., & Kulp, M. (2009). *Louisiana Barrier Island Comprehensive Monitoring Program (BICM) Volume 2*: Shoreline Changes and Barrier Island Land Loss 1800's-2005. http://scholarworks.uno.edu/pies_rpts/1

McBride, R. A., & Byrnes, M. R. (1997). Regional variations in shore response along barrier island systems of the Mississippi River delta plain: historical change and future prediction. *Journal of Coastal Research*, 628-655. https://www.jstor.org/stable/4298660

McBride, R. A., Byrnes, M. R., & Hiland, M. W. (1995). Geomorphic response-type model for barrier coastlines: a regional perspective. *Marine Geology, 126*(1-4), 143-159. https://doi.org/10.1016/0025-3227(95)00070-F

McBride, R. A., Penland, S., Hiland, M. W., Williams, S. J., Westphal, K. A., Jaffe, B .E., & Sallenger, A. H., Jr. (1992). Analysis of barrier shoreline changes in Louisiana from 1853 to 1989. In: Williams, S. J.; Penland, S., & Sallenger, A. H., Jr., (Eds), Louisiana Barrier Island Erosion Study-Atlas of Barrier Shoreline Changes in Louisiana from 1853 to 1989. *US. Geological Survey Misc. Invest. Series I-2150-A,* pp. 36-97

Meyer-Arendt, K. J. (1985). The Grand Isle, Louisiana resort cycle. *Annals of Tourism Research, 12*(3), 449-465. https://doi.org/10.1016/0160-7383(85)90009-X

Miner, M. D., Kulp, M. A., FitzGerald, D. M., Flocks, J. G., & Weathers, H. D. (2009). Delta lobe degradation and hurricane impacts governing large-scale coastal behavior, south-central Louisiana, USA. *Geo-Marine Letters*, *29*(6), 441-453. doi: 10.1007/s00367-009-0156-4.

Missimer, T. M. (1973). Growth rates of beach ridges on Sanibel Island, Florida. *Gulf Coast Association of Geological Societies Transactions, 23*, 383-388.

Moore, L. J., Jol, H. M., Kruse, S., Vanderburgh, S., & Kaminsky, G. M. (2004). Annual layers revealed by GPR in the subsurface of a prograding coastal barrier, southwest Washington, USA. *Journal of Sedimentary Research*, *74*(5), 690-696. https://doi.org/10.1306/021604740690

Morang, A., Rosati, J. D., & King, D. B. (2013). Regional sediment processes, sediment supply, and their impact on the Louisiana coast. *Journal of Coastal Research*, *63*(sp1), 141-165. https://doi.org/10.2112/SI63-013.1

Morgan, J. P., & Conatser, W. E. (1971). The Lafourche Delta and the Grand Isle barrier island: Destruction of a ancient delta of the Mississippi River. New Orleans Geological Society Field Trip.

Murray, A. S. & Wintle, A. G. (2000). Luminescence dating of quartz using an improved single-aliquot regenerative-dose protocol. *Radiation measurements*, *32*(1), 57-73. https://doi.org/10.1016/S1350-4487(00)00089-5

Murray-Wallace, C. V., Banerjee, D., Bourman, R. P., Olley, J. M., & Brooke, B. P. (2002). Optically stimulated luminescence dating of Holocene relict foredunes, Guichen Bay, South Australia. *Quaternary Science Reviews*, *21*(8-9), 1077-1086. https://doi.org/10.1016/S0277-3791(01)00060-9

Neal, A. (2004). Ground-penetrating radar and its use in sedimentology: principles, problems and progress. *Earth-science reviews, 66*(3-4), 261-330. https://doi.org/10.1016/j.earscirev.2004.01.004

Neal, A., & Roberts, C. L. (2000). Applications of ground-penetrating radar (GPR) to sedimentological, geomorphological and geoarchaeological studies in coastal environments. Geological Society, London, *Special Publications, 175*(1), 139-171. https://doi.org/10.1144/GSL.SP.2000.175.01.12

Nielsen, A., Murray, A. S., Pejrup, M., & Elberling, B. (2006). Optically stimulated luminescence dating of a Holocene beach ridge plain in Northern Jutland, Denmark. *Quaternary Geochronology*, *1*(4), 305-312. https://doi.org/10.1016/j.quageo.2006.03.001

Nienhuis, J. H., Törnqvist, T. E., Jankowski, K. L., Fernandes, A. M. & Keogh, M. E. (2017). A new subsidence map for coastal Louisiana. *GSA Today*, *27*(9), 58-59.

Nieuwenhuyse, A., Jongmans, A. G., & Van Breemen, N. (1994). Mineralogy of a Holocene chronosequence on andesitic beach sediments in Costa Rica. *Soil Science Society of America Journal*, *58*(2), 485-494. doi:10.2136/sssaj1994.03615995005800020034x.

Olhoeft, G. R. (2002). Applications and frustrations in using ground penetrating radar. *IEEE aerospace and electronic systems magazine*, *17*(2), 12-20. doi: 10.1109/62.987130.

Oliver, T. S., Dougherty, A. J., Gliganic, L. A., & Woodroffe, C. D. (2015). Towards more robust chronologies of coastal progradation: optically stimulated luminescence ages for the coastal plain at Moruya, south-eastern Australia. *The Holocene*, *25*(3), 536-546. https://doi.org/10.1177/0959683614561886

Otvos, E. G. (2000). Beach ridges—definitions and significance. *Geomorphology, 32*(1), 83-108. https://doi.org/10.1016/S0169-555X(99)00075-6

Penland, S., Boyd, R., & Suter, J. R. (1988). Transgressive depositional systems of the Mississippi delta plain: a model for barrier shoreline and shelf sand development. *Journal of Sedimentary Research, 58*(6), 932-949. https://doi.org/10.1306/212F8EC2-2B24-11D7-8648000102C1865D

Penland, S., & Ramsey, K. E. (1990). Relative sea-level rise in Louisiana and the Gulf of Mexico: 1908-1988. *Journal of Coastal Research*, 323-342. https://www.jstor.org/stable/4297682

Penland, S., Ritchie, W., Boyd, R., Gerdes, R. G., & Suter, J. R. (1986). The Bayou Lafourche delta, Mississippi River delta plain, Louisiana. *South-Eastern Section of the Geological Society of America: Decade of North American Geology, Centennial Field Guide Volume 6*(6), 447.

Penland, S., Suter, J. R., & Boyd, R. (1985). Barrier island arcs along abandoned Mississippi River deltas. *Marine Geology, 63*(1-4), 197-233.

Penland, S., Williams, S. J., Davis, W. D., Sallenger, A. H. & Groat, C. G. (1992). "Barrier Island Erosion and Wetland Loss in Louisiana" in *Atlas of Shoreline Changes in Louisiana from 1853 to 1989* (p. 7). Reston, Virginia: US Geological Survey.

Prescott, J. R., & Hutton, J. T. (1988). Cosmic-ray and gamma-ray dosimetry for TL and electron-spin-resonance. *Nuclear Tracks and Radiation Measurements, 14*, 223–227.

Prescott, J. R., & Hutton, J. T. (1994). Cosmic ray contributions to dose rates for luminescence and ESR dating: Large depths and long-term time variations. *Radiation Measurements, 23,* 497–500.

Psuty, N. P. (1965). Beach-ridge development in Tabasco, Mexico. *Annals of the Association of American Geographers, 55*(1), 112-124.

Rémillard, A. M., Buylaert, J. P., Murray, A. S., St-Onge, G., Bernatchez, P., & Hétu, B. (2015). Quartz OSL dating of late Holocene beach ridges from the Magdalen Islands (Quebec, Canada). *Quaternary Geochronology, 30*, 264-269. https://doi.org/10.1016/j.quageo.2015.03.013

Rey, T., Lefevre, D., & Vella, C. (2009). Deltaic plain development and environmental changes in the Petite Camargue, Rhone Delta, France, in the past 2000 years. *Quaternary Research*, *71*(3), 284-294. https://doi.org/10.1016/j.yqres.2008.10.007

Rink, W. J., & Forrest, B. (2005). Dating evidence for the accretion history of beach ridges on Cape Canaveral and Merritt Island, Florida, USA. *Journal of Coastal Research*, 1000-1008. https://doi.org/10.2112/03-0058.1

Rink, W. J., & Lopez, G. I. (2010). OSL-based lateral progradation and aeolian sediment accumulation rates for the Apalachicola Barrier Island Complex, North Gulf of Mexico, Florida. *Geomorphology, 123*(3-4), 330-342. https://doi.org/10.1016/j.geomorph.2010.08.001

Roberts, H. H., Huh, O. K., Hsu, S. A., Rouse, L. J., & Rickman, D. (1987, May). Impact of cold-front passages on geomorphic evolution and sediment dynamics of the complex Louisiana coast. In *Coastal Sediments* (pp. 1950-1963). ASCE.

Rodnight, H. (2008). How many equivalent dose values are needed to obtain a reproducible distribution? *Ancient Thermoluminescence, 26*, 3–9.

Savage, R. P. (1959). Notes on the formation of beach ridges. *Bulletin of Beach Erosion Board, 13,* 31-35.

Scheffers, A., Engel, M., Scheffers, S., Squire, P. and Kelletat, D. (2012). Beach ridge systems–archives for Holocene coastal events?. *Progress in Physical Geography, 36*(1), 5-37. https://doi.org/10.1177/0309 133311419549

Shepard, F. P., & Young, R. (1961). Distinguishing between beach and dune sands. *Journal of Sedimentary Research, 31*(2).

Short, M. A., & Huntley, D. J. (1992). Infrared stimulation of quartz. *Ancient Thermoluminescence, 10,* 19–21.

Stapor Jr, F. W., Mathews, T. D., & Lindfors-Kearns, F. E. (1991). Barrier-island progradation and Holocene sea-level history in southwest Florida. *Journal of Coastal Research*, 815-838. https://www.jstor.org/stable/4297898

Stone, G. W., Grymes III, J. M., Dingler, J. R., & Pepper, D. A. (1997). Overview and significance of hurricanes on the Louisiana coast, USA. *Journal of Coastal Research*, 656-669. https://www.jstor.org/stable/4298661

Stone, G. W., Stapor Jr, F. W., May, J. P., & Morgan, J. P. (1992). Multiple sediment sources and a cellular, non-integrated, longshore drift system: Northwest Florida and southeast Alabama coast, USA. *Marine Geology, 105*(1-4), 141-154. https://doi.org/10.1016/0025-3227(92)90186-L

Stutz, M. L., & Pilkey, O. H. (2001). A review of global barrier island distribution. *Journal of Coastal Research,* 15-22. https://www.jstor.org/stable/25736270

Syvitski, J. P., Kettner, A. J., Overeem, I., Hutton, E. W., Hannon, M. T., Brakenridge, G. R., Day, J., Vörösmarty, C., Saito, Y., Giosan, L. & Nicholls, R. J. (2009). Sinking deltas due to human activities. *Nature Geoscience*, *2*(10), p.681. doi:10.1038/ngeo629.

Tamura, T. (2012). Beach ridges and prograded beach deposits as palaeoenvironment records. *Earth-Science Reviews*, *114*(3-4), 279-297. https://doi.org/10.1016/j.earscirev.2012.06.004

Tamura, T., Ito, K., Inoue, T., & Sakai, T. (2017). Luminescence dating of Holocene beach-ridge sands on the Yumigahama Peninsula, western Japan. *Geochronometria, 44*(1), 331-340. http://www.degruyter.com/view/j/geochr

Tamura, T., Murakami, F., Nanayama, F., Watanabe, K., & Saito, Y. (2008). Ground-penetrating radar profiles of Holocene raised-beach deposits in the Kujukuri strand plain, Pacific coast of eastern Japan. *Marine Geology*, *248*(1-2), 11-27. https://doi.org/10.1016/j.margeo.2007.10.002

Tanner, W. F. (1971). Growth rates of Venezuelan beach ridges. *Sedimentary Geology*, *6*(3), 215-220. https://doi.org/10.1016/0037-0738(71)90037-6

Taylor, M., & Stone, G. W. (1996). Beach-ridges: a review. *Journal of Coastal Research*, 612-621. https://www.jstor.org/stable/4298509

Theis, A. R. (1969). Beach Erosion Problems at Grand Isle, Louisiana. *Shore and Beach, 37*(1), 19-22.

van Heteren, S., Fitzgerald, D. M., Mckinlay, P. A., & Buynevich, I. V. (1998). Radar facies of paraglacial barrier systems: coastal New England, USA. *Sedimentology, 45*(1), 181-200. https://doi.org/10.1046/j.1365-3091.1998.00150.x

Vespremeanu-Stroe, A., Preoteasa, L., Zăinescu, F., Rotaru, S., Croitoru, L., & Timar-Gabor, A. (2016). Formation of Danube delta beach ridge plains and signatures in morphology. *Quaternary International*, *415*, 268-285. https://doi.org/10.1016/j.quaint.2015.12.060

Visher, G. S. (1969). Grain size distributions and depositional processes. *Journal of Sedimentary Research, 39*(3).

Williams, S. J., Penland, S., & Sallenger, A. H. (1992). *Atlas of Shoreline Changes in Louisiana from 1853 to 1989* (p. 103). Reston, Virginia: US Geological Survey.

Wintle, A. G. & Murray, A. S. (2006). A review of quartz optically stimulated luminescence characteristics and their relevance in single-aliquot regeneration dating protocols*. Radiation measurements, 41*(4), pp.369-391. https://doi.org/10.1016/j.radmeas.2005.11.001

APPENDIX

1. Beach ridge geometric analysis

The spacing between adjacent ridges was measured using the *Google Earth Pro* measure tool and recorded and on the basis of these measurements and subsequently split into Groups I and II (Tables A1.1 and A1.5). Two-sample T-Tests assuming unequal variances were conducted in *Microsoft Excel* to determine whether there are any significant differences in spacing and geographic orientation between and within groups and sets (Table A1.2). The lagoonward ends, or terminations, of the beach ridges in Group I are all that currently exist; the shafts (or midsections) and origins of these ridges have been reworked and therefore the geomorphologic characteristics could not be measured. For those ridges in Group II, measurements of spacing were taken between the origins, the center of the shafts, and the terminal ends. The null hypothesis in all cases is that there is no difference in spacing for those ridges being compared.

Differences in azimuth bearing of ridges can provide information about the primary direction of progradation and other details about growth patterns. The same measurement techniques described above were used to measure the bearings of the lagoonward tips of all beach ridges (Tables A1.3 and A1.6). T-tests were conducted to determine whether there are any significant differences between or within groups and sets (Table A1.4). The null hypothesis in all cases is that there is no difference in bearings for those ridges being compared.

Set 1		Set 2		Set 3	
Space	Distance (m)	Space	Distance (m)	Space	Distance (m)
1	55.82	21	65	34	125.79
2	78.8	22	74.74	35	57.48
3	88.37	23	63.16	36	60.82
4	54.64	24	69.78	37	31.14
5	49.86	25	41.83	38	44.07
6	68.31	26	117.86	39	82.41
7	55.38	27	99.32	40	46.5
8	64.58	28	152.31	41	59.59
9	50.73	29	118.33	42	60.86
10	50.62	30	76.03	43	120.31
11	38.77	31	71.61	44	65.63
12	70.03	32	49.05	45	58.18
13	75.18	33	78.25	46	72.76
14	92.64	34	125.79	47	63.15
15	50.62 σ		30.76788	48	50.61
16	85.81		σ		25.01097
17	31.99				
18	114.55				
19	24.43				
20	43.66				
σ	21.66338				

Table A1.1. The spacing between adjacent ridge segments among Sets 1-3.

	Set 1	Set 2		Set 1	Set 3		Set 2	Set 3
Mean	62.24	85.93	Mean	62.24	66.62	Mean	85.9	66.62
Variance	494	1019	Variance	494.0	670.2	Variance	1019.5	670.2
Observations	20	14	Observations	20	15	Observations	14	15
Hypothesized Mean Difference	0		Hypothesized Mean Difference	0		Hypothesized Mean Difference	0	
df	22		df	28		df	25	
t Stat	-2.40		t Stat	-0.525		t Stat	1.78	
P(T<=t) one-tail	0.012	Reject H_o	P(T<=t) one-tail	0.302	Accept H_o	P(T<=t) one-tail	0.0434	Reject H_o
t Critical one-tail	1.72		t Critical one-tail	1.70		t Critical one-tail	1.71	
P(T<=t) two-tail	0.03		P(T<=t) two-tail	0.60		P(T<=t) two-tail	0.09	
t Critical two-tail	2.07		t Critical two-tail	2.05		t Critical two-tail	2.06	

Table A1.2. Spacing values for Sets 1-3 were compared to determine if any significant differences exist using two-sample T-tests (assuming unequal variances).

2. Ground penetrating radar

2.1 Acquisition

Nineteen approximately shore-perpendicular GPR profiles were acquired across the using a *MALÅ* push-cart system with a 250 MHz antenna. The soil velocity was set to 0.172 m/ns when the GPR was acquired, the upper limit of the velocity range for asphalt as well as dry sand (Johnson et al., 1979). However, other materials, such as soil, wet sand, and concrete were also materials through which the waves had to propagate, so two lines were repeated at a later date, once with the soil velocity set to 0.06 m/ns (which corresponds to the velocity ranges for wet sandy soil, concrete, and saturated sand; Johnson et al., 1979) and again at 0.15 m/ns, which corresponds to dry sand and freshwater (Davis & Annan, 1989).

With the exception of the two transects acquired along roads within Grand Isle State Park at the northeast end of the island, profiles were collected along existing paved residential streets. All began along the backside of the island and extend to the beach in most cases; several transects terminate just before the beach due to weather conditions and private property boundaries. Additionally, two NE-SW trending profiles were acquired approximately perpendicular to the others. The lengths of the 21 profiles range from 1,100 m near the northeastern end of the island to 325 m in the southwest.

Profiles were acquired on three different occasions, each chosen because these days followed intense rain events. The dielectric permittivity, conductivity and velocity of fresh water causes GPR to work well in this media. Despite the proximity to the Gulf, and the potential for subsurface large volumes of conductive, saline water, GPR can work extremely well in coastal sediments if there is a freshwater lens. Leatherman (1983) reviewed potential applications for GPR in coastal sediments, and Neal and Roberts (2000) provide a good review of subsequent progress. GPR studies of spits and barrier beaches (Jol et al., 1996a; Van Heteren et al., 1998; Smith et al. 1999) and a prograding foreland (Neal & Roberts 2000) show good resolution of large-scale sedimentary structures from prograded shorefaces (Bristow & Jol, 2003).

Grand Isle is a highly developed island with little natural landscape remaining. Buildings and private property boundaries restricted GPR transects to existing streets. As a result, most lines were saturated with noise. The different types of noise identified during this investigation are summarized in figure A2.1.

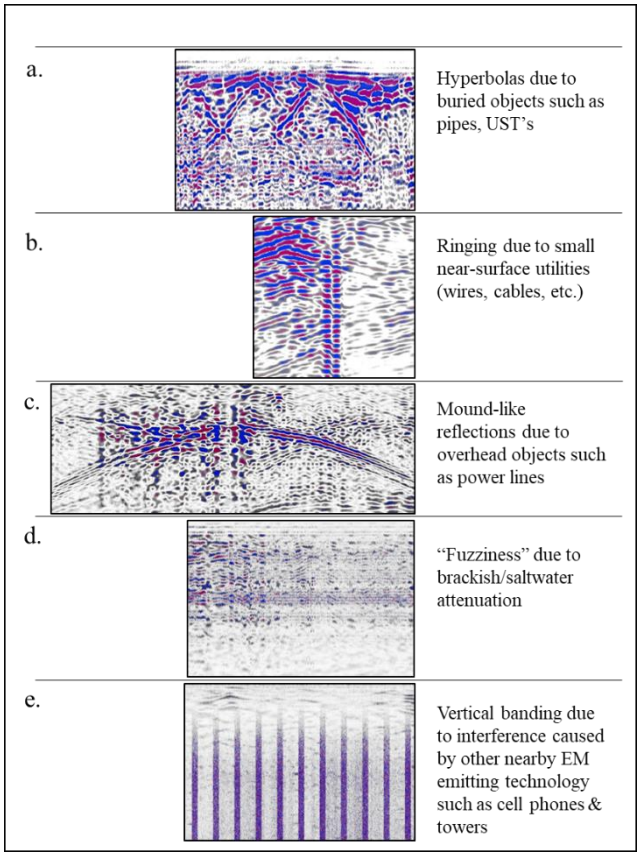

Figure A2.1. The five types of noise encountered in many of the radargrams.

2.2 Processing

The data in its raw form is unsuitable for interpretation (Fig. A2.2). The 2D GPR profiles underwent an initial processing procedure in *GPRSoft* by Geoscanners AB. The main objective of processing the data is to provide more noise free and cleaner data that facilitates the geometry and extent of subsurface reflectors . The processing steps used for all lines of this study were:

1) A temporal running average filter was applied to remove very low frequency components, commonly referred to as "de-wowing" the data. This step applies a running average filter to each trace to remove the initial DC signal component, low frequency "wow" caused by signal saturation due to early wave arrivals, inductive coupling effects, and/or instrumentation dynamic range limitations, and filter out inherent, nonlinear, low-frequency noises associated with antenna characteristics (Jol, 2008).

2) Custom gains were applied to amplify the signal and reflectors at depth. It relies upon user-defined limits and is inversely proportional to signal strength, and therefore attempts to equalize all signals (Jol & Bristow, 2003; Jol, 2008).

3) Surface correction was used to set the time zero position relative to the ground surface;

4) Background or noise removal was applied, which first calculates an average of the background noise depending on the input parameters and then subtracts the resulting trace from every trace in the profile (Kim et al., 2007).

5) A single pass of an IIR band pass filter was applied using user-specified high pass and low pass boundaries.

6) Application of more gain if deemed necessary.

7) A migration adaptation tool was used to collapse diffractions. In this software the velocity value was adjusted and then used to apply the migration to the data. Hyperbolas collapsing into dots was an indication that the correct velocity had been selected. Transformation of the hyperbolas turn into concave up signature was an indication that the selected velocity was too high, and if the hyperbolas remained hyperbolas then the velocity is too low (*GPRSoft* User Guide, 2011).

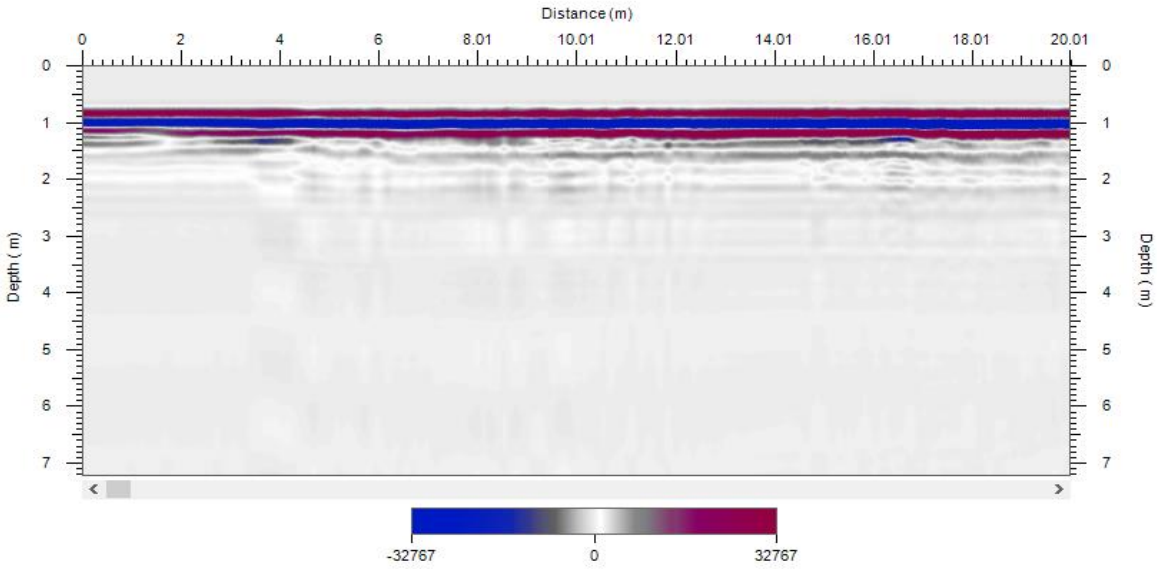

Figure A2.2. The GPR data in its raw form is unsuitable for interpretation.

3. Volumetric and rate calculations

3.1 Lithosome volume calculations

Inventory and examination of all preexisting sedimentary and stratigraphic data for the island was conducted in order to approximate the 3-D geometry and volume of the uppermost sand body. A combination of Conatser's (1971) isolith map for the "A" sand, the strike-aligned cross section from Kulp et al. (2005), and shore-perpendicular cross sections prepared by Dunbar et al. (1994) and Fisk (1955), were used. First, the horizontal extent of the sand body was divided into 0.09 km^2 boxes (each side of the square = 0.3 km). Each box was then assigned a thickness value between one and 9 m. The number of boxes in each of the nine thickness categories was multiplied by the area of a box and by the box thickness to give a volume for each category (Fig. A3.1). The volume of the Grand Isle barrier lithosome is represented by

$$\text{and} \quad \sum_{i=1}^{9} X_i y_i (0.09)$$

where x = thickness in meters
y = number of occurrences

The Grand Isle barrier lithosome calculated here is 92,610,000 m^3 (Table 3.5). In order to determine the rate at which sediment must be supplied to the island, the calculated volume was divided by 0.75 kyr, an estimated time since the formation of Grand Isle. An average of approximately 123,467 m^3/yr must have been available to the island during the period of its formation.

The same procedure was conducted for the "B" sand of Conaster (1971). See figure A3.2.

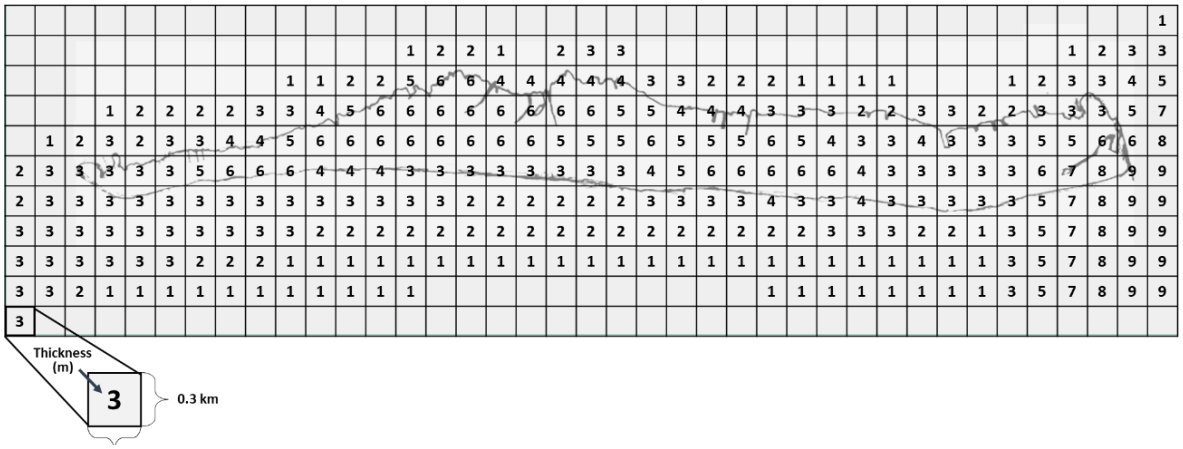

Fig. A3.1. Using Conatser's (1971) isolith map, an approximate volume of the "A" sand was calculated. Each sand body was divided into equally-sized squares of a known dimension that were assigned thickness values which were then combined for an approximate total volume.

3.2 Sediment transport and deposition rate calculations

One goal of this study was to determine the approximate rate at which the Caminada headland eroded and supplied sand to Grand Isle during the past 750 yrs. The abandoned delta and beach ridge

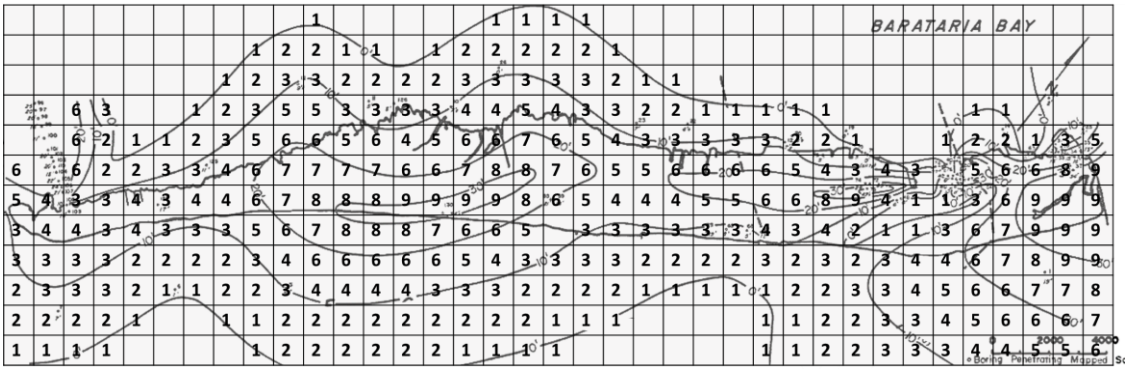

Fig. A3.2. Using Conatser's (1971) isolith map, an approximate volume of the "B" sand was calculated. Each sand body was divided into equally-sized squares of a known dimension that were assigned thickness values, which were then combined for an approximate total volume.

plain headland have eroded landward more than 2 km in the central headland since the 1880s at an average rate of about 13.4 m^2/yr (McBride et al., 1992). Volumetrically, between 1880 and 2006, the Caminada headland and its shoreface to water depths greater than -10 m has lost 10,500,000 m^3 (Miner et al., 2009). Based on sediment budget calculated by Harper (1977) through a quantitative analysis of aerial photographs from 1952 and map overlays from 1972 and 1957, less than 5% of the volumetric loss of the Caminada headland is redeposited back onto the Caminada headland. Moreover, most of this redeposition is typically in the form of washover fans and within recurved spits and does not directly renourish the beaches and shoreface adjacent to areas of erosion. 41% of the sediment (230,000 m^3/yr) eroded off the Caminada headland has been suggested to be captured along the western edge of the Barataria Pass Jetty; which means that the same amount (230,000 m^3/yr) if not twice as much must pass through Caminada Pass and eventually make its way to Grand Isle and Barataria Pass due to longshore transport (Harper, 1977). Longshore sediment transport rates from the Caminada headland west of Grand Isle to Grand Pass, the second inlet east of Grand Isle, have also been estimated by Georgiou et al. (2005) at 146,000 m^3/yr.

Diversion of the longshore current occurs near the boundary of the eastern two-thirds of the headland; therefore, this study is only concerned with the eastern 60% of the headland. For this study only sand-sized material that composes the bulk of Grand Isle was considered. Where appropriate, volumetric figures were adjusted for sand content only. Four different rates of Caminada headland erosion were calculated using a combination of multiple sources (1-4 below). An additional two rates were retrieved from the literature for comparisons (5 and 6 below). Each is described below.

1. An average shoreface volume change per year (10,600,000 m^3/yr) for an approximately 70 km study area including the headland was calculated from those from three different time periods provided in Georgiou et al. (2010; Fig. 3.3): -9.43x10^6 m^3/yr (1880-1930), -11x106 m^3/yr (1930-1980), and -11.54x10^6 (1980-2007). The area of interest (eastern Caminada headland) constitutes only 14 km, or 20% of the total study area, which yields 2,121,000 m^3/yr for the area of interest. This rate includes all sediment sizes, only 14% of which is estimated to be sand by

Geomorphic unit	Volume change per year (1880 - 1930) (10^6 m^3 yr^{-1})	Volume change per year (1930 - 1980) (10^6 m^3 yr^{-1})	Volume change per year (1980 - 2007) (10^6 m^3 yr^{-1})
Backbarrier	0.78	-0.09	-0.29
Ebb Tidal Delta	0.41	2.03	-0.49
Shoreface	-9.43	-11.00	-11.54
Spit Platform	0.00	0.08	0.01
Tidal Inlet	-0.18	-0.73	-0.05

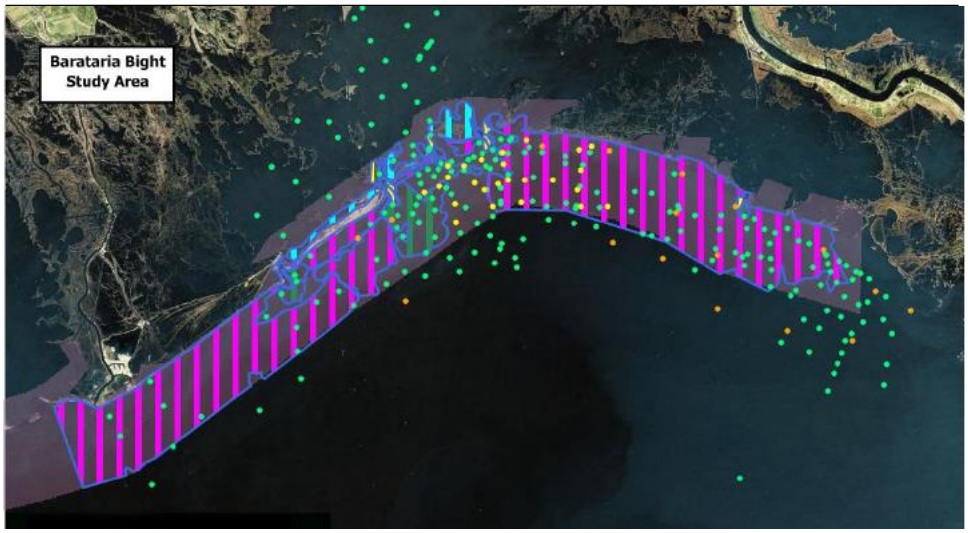

Fig A3.3. An average of the shoreface values for the three time periods was used in method 1. The area of interest for this study is 20% of the study area in Georgiou et al. (2010).

the authors. This gives a final shoreface (subaqueous) erosion rate of 296,940 m^3/yr. The subaerial portion was calculated from values provided by McBride et al. (1992; Fig. A3.4). Along the same 14 km of shoreline used above, there was a shoreline retreat rate of -10.8 m/yr, only approximately half of which is land composed of sandy beach ridges. A shoreline length of 7 km was used to give an average surface area rate of erosion of 75,600 m^2/yr. To get a volumetric rate of erosion, an average elevation of the study area surface of 0.5 m was used to give 37,800 m^3/yr. Finally, the subaqueous rate (296, 940 m^3/yr) and the subaerial rate (37,800 m^3/yr) were added for a total of 334,740 m^3/yr.

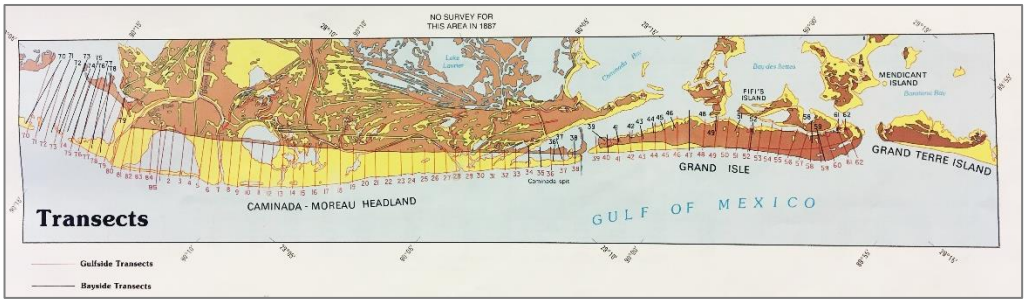

Transect	1887-1934	1934-1956	1956-1978	1978-1988	1887-1988	Change in 720yr
12	861	418	-528	128	1935	13932
13	815	727	-194	151	1887	13586
14	848	546	-254	215	1863	13414
15	855	582	-167	233	1837	13226
16	818	373	-272	254	1717	12362
17	806	367	-249	253	1675	12060
18	748	332	-234	420	1734	12485
19	659	287	-237	213	1396	10051
20	538	278	-213	190	1219	8777
21	528	243	-212	189	1172	8438
22	490	201	-253	167	1111	7999
23	433	187	-250	164	1034	7445
24	423	165	-263	150	1001	7207
25	386	292	-122	139	939	6761
26	405	246	-164	144	959	6905
27	386	228	-187	120	921	6631
28	352	175	-212	117	856	6163
29	379	306	-77	79	841	6055
30	410	293	-30	81	814	5861
31	395	125	-169	52	741	5335
32	461	94	-133	52	740	5328
33	433	85	-96	50	664	4781
34	423	111	-28	63	625	4500
35	439	87	35	52	543	3910
36	398	82	15	28	493	3550
37	378	62	40	28	428	3082
38	265	0	4	35	296	2131
Total:	14332	6892	-4450	3767	29441	
Average:	530.81481	255.25926	-164.8148	139.51852	1090.407	

Fig. A3.4. Transects 12-38 were used in the calculation of subaerial erosion of the eastern Caminada headland. From McBride et al. (1992; above). Transects were used to project the seaward extent of the Caminada headland at 700 yr BP. The magnitudes of shoreline retreat for each transect for the period 1887-1988 were multiplied by 6 to give an approximation of how far the shoreline would have protruded into the Gulf at 0.7 ka.

2. Harper (1977) provides volumetric erosion rates for the Caminada headland for the period of 1952-1972 (Table A3.3). Harper assumes all sediment eroded from the headland is carried northeastward at a rate of 305,950 m^3/yr. The author also provides an estimate of 41% of eroded sediment reaching and contributing to the aggradation of Grand Isle. This rate is considered conservative because although it accounts for subaerial and subaqueous erosion, the author uses a depth of erosion that includes most, but not all, of sediment actually eroded from the shoreface.

3. Miner et al. (2009) calculated a net change in the volume of the Caminada headland shoreface between 1880 and 2006 of -1.051x10^9 m^3, or 8.342x10^6 m^3/yr. When the same constraints are applied to this annual rate as was identified in method 1 (20% of study area and 14% sand-sized material), it generates a rate of 233,576 m^3/yr. To this value, the subaerial volumetric erosion from method 1 (75,600 m^3/yr) is added to provide a final rate of 309,176 m^3/yr.

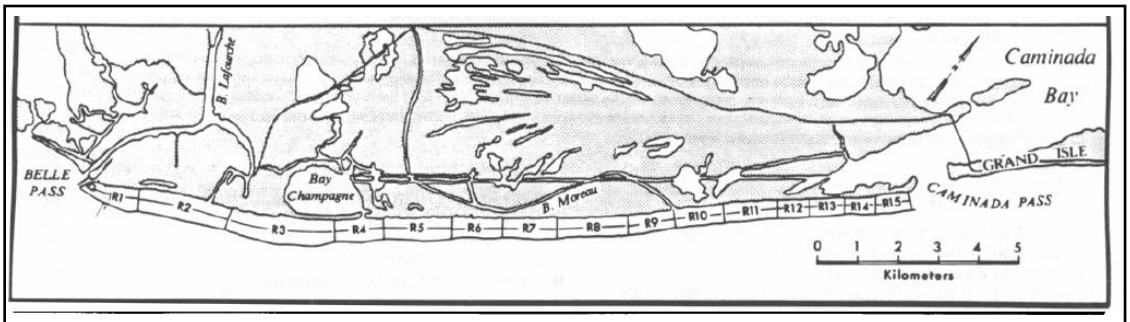

Range	Depth Erosion (m)	Linear Changes (m)		Areal Changes (m² x 10³)		Volumetric Changes (m³ x 10⁴)		(m³ x 10³/km)
	1952-1972	1952-1972	Annual	1952-1972	Annual	1952-1972	Annual	Annual
R- 1	6.1	- 61	- 3.0	- 74.1	- 3.7	- 452.	- 23.0	-19.
R- 2	4.3	-122	- 6.1	-307.0	-15.4	-1320.	- 66.0	-26.
R- 3	5.8	-304	-15.2	-470.0	-23.5	-2724.	-136.0	-61.
R- 4	5.8	-365	-18.5	- 94.9	- 4.7	- 550.	- 28.0	-19.
R- 5	5.2	-213	-10.6	-130.0	- 6.5	- 675.	- 34.0	-21.
R- 6	4.6	-183	- 9.2	-192.0	- 9.6	- 884.	- 44.0	-33.
R- 7	5.5	-152	- 7.6	-227.0	-11.4	- 818.	- 41.0	-25.
R- 8	4.6	-183	- 9.2	-263.0	-13.2	-1208.	- 60.0	-37.
R- 9	5.5	-183	- 9.2	-165.0	- 8.2	- 909.	- 45.0	-36.
R-10	5.5	-140	- 7.0	- 75.1	- 3.8	- 413.	- 21.0	-16.
R-11	5.2	-137	- 6.8	-115.0	- 5.8	- 597.	- 30.0	-24.
R-12	5.5	- 91	- 4.6	- 13.7	- 1.4	- 350.	- 18.0	-20.
R-13	4.6	- 76	- 3.8	+ 22.3	+ 2.2	- 69.	- 3.0	- 4.
R-14	4.0	—	—	+238.0	+11.9	+ 238.	+ 12.0	+13.
R-15	4.3	+ 76	+3.8	+ 75.6	+ 3.8	+ 116.	+ 1.2	+ 7.

Table A3.5. The Caminada headland erosion rates along 15 shore-normal transects reported by Harper (1977) used to calculate the potential sediment flux to Grand Isle in method 2.

4. List et al. (1994) mapped bathymetric changes along the Caminada headland between 1878-1989 (Fig. A3.6). Here the cross-sectional areas of two transects (M-M' and N-N') were calculated from both ends of the study area, which were then multiplied by the alongshore distance of the study area (14,000 m). The two resulting volumes were then multiplied by 0.14 sand content and then divided by the study length, age difference of the two transects (111 yrs). The calculated rates of erosion for transect M-M' (307,243 m^3/yr) and N-N' (123,603 m^3/yr) were averaged and added to the subaerial erosion rate calculated from McBride et al. (1992) for a final rate of 291,023 m^3/yr.

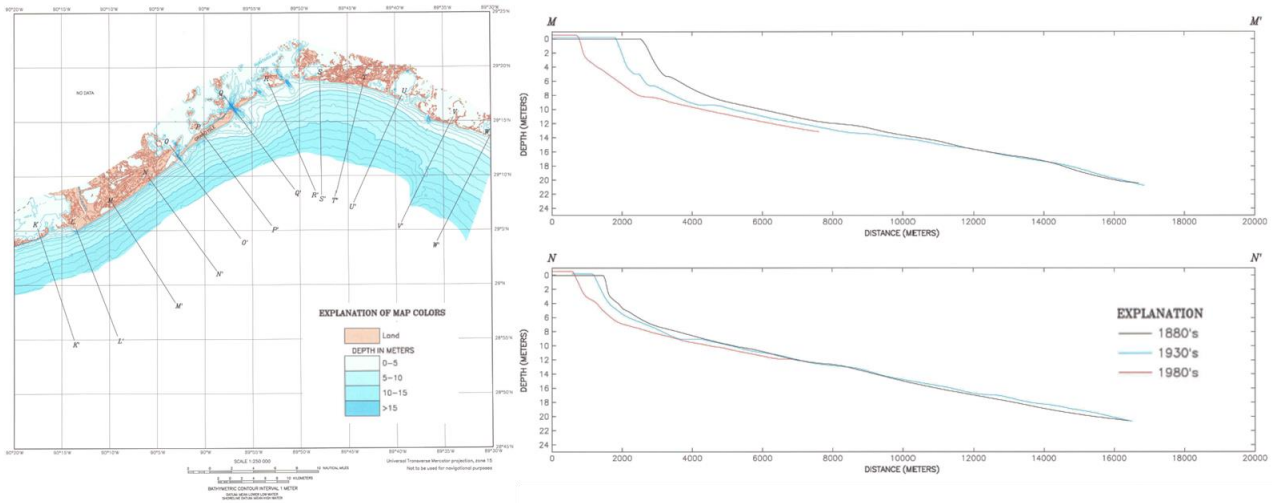

Fig. A3.6. The bathymetric profiles used to calculate shoreface erosion rates for method 6 and their locations along the Caminada headland. From List et al. (1994).

5. Morang et al. (2013) provides a sediment budget for the Caminada headland area (Fig. A3.7). Although it shows no sediment being transported directly to Grand Isle from the headland, the diagram shows residual of -191,000 m^3/yr for Grand Isle, indicating that this amount of sediment reaches the island, but does not specify the source.

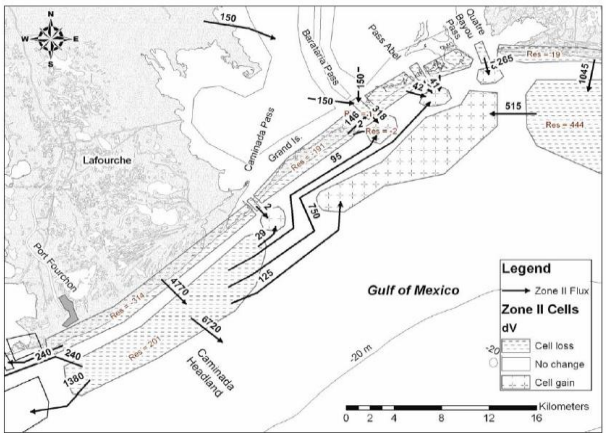

Fig. A3.7. The sediment budget calculated by Morang et al. (2013). Although no sediment is being transported directly to Grand Isle, the island shows a residual of -191,000 m^3/yr.

6. Georgiou et al. (2005) concluded that 146,000 m^3/yr of sediment moves northeastward from the eroding headland, any/all of which is available for deposition at Grand Isle. See figure A3.8.

4. Optically stimulated luminescence sediment dating and growth rate calculations

4.1 Sample collection

Five OSL samples were collected, each from a different beach ridge set. Sample sites were chosen in order to assure representation from as many ridge sets as possible. Potential sites were

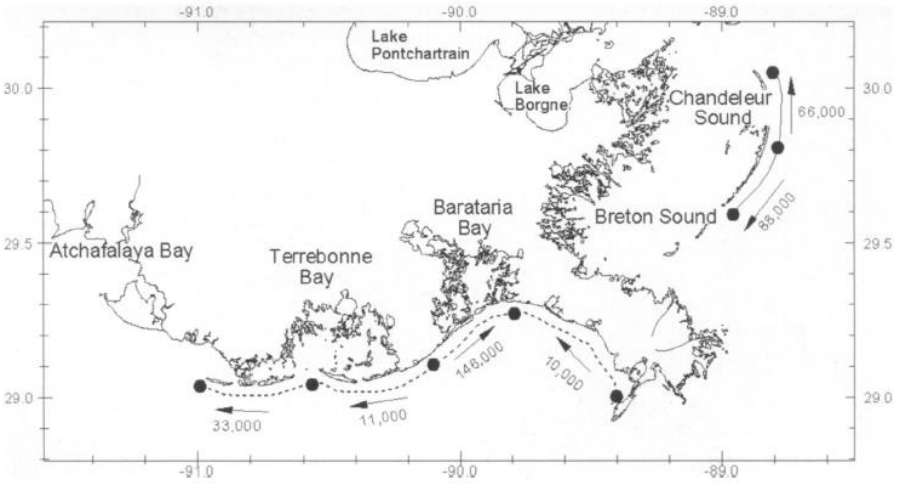

Fig. A3.8. Longshore sediment transport rates in cubic meters per year reported by Georgiou et al. (2005). 146,000 m^3/yr is being transported from the Caminada headland eastward toward Grand Isle.

limited as the island is heavily developed and OSL analysis is most reliable when samples are collected from undisturbed sediments. For four out of the five samples, trenches reached the water table just above or at one-meter depth. Emptied and cleaned steel food cans were inserted horizontally into the vertical wall of the trench at 80 to 100 cm depth, depending on where the water table was encountered. The cans were pressed into the sediment until full penetration, and then carefully turned and extracted. Open can ends were capped with plastic caps and sealed with several layers of duct tape and labelled. The samples were analyzed at North Dakota State University's Optical Dating and Dosimetry Lab in Fargo, ND.

4.2 Analysis

All OSL samples were processed and measured in the Optical Dating and Dosimetry Lab at North Dakota State University under controlled lighting conditions (Na-vapor lamps). After discarding the exposed ends of the sample canister, the sediment was sieved to obtain sand, in the 150 to 250 µm size fraction (fine-grained sand). Clean quartz was then separated by typical luminescence dating preparation procedures, which include digestion of organic matter by H_2O_2, dissolution of carbonates with HCl, and aggressive treatment with HF acid to etch quartz grains surfaces and breakdown feldspars. Followed by HCl and Na-pyrophosphate rinses to remove precipitates and particulates (Aitken, 1998). After drying, the clean quartz sand grains were attached to aliquots for OSL measurements using a non-luminescent medical adhesive. The purity of the processed quartz sands was verified by infrared prescreening (Short and Huntley, 1992).

All measurements and irradiations were conducted using a Risø DA-15 automated TL/OSL reader system. The system is equipped with a 90Sr/90Y ß-source for dose calibrations, which irradiated at a rate of 0.113 Gy/s. Luminescence was stimulated with blue light (470 ± 30 nm) from a diode array and

measured with an EMI model 9235QA PMT in the UV emission range (5 mm Hoya U-340). Data was collected following the OSL single aliquot regeneration (SAR) procedures of Murray and Wintle's (2000) with the minor modification of maintaining uniform cut-heat and preheat treatments of 160˚C for 10 s (Lepper et al., 2000; Wintle & Murray, 2006) and using a relatively large test dose because of the youthfulness of the samples (Lepper et al., 2017). Four regeneration doses were used as well as a fifth midpoint regeneration dose, or check dose (Dc), to assess the fidelity of dose recovery (Lepper et al., 2000). Check dose analysis is also used as part of the data filtering process described in Lepper et al. (2003). Dose response calibration was conducted for every aliquot and equivalent doses (De) were interpolated by linear local slope approximation. De data was collected from 96 individual subsamples (aliquots) from each field sample providing data set ranging in size from 91 to 95 Des after filtering (Table A4.1). The use of over 50 aliquots/Des from each sample leads to increased precision of individual ages (Rodnight, 2008).

Dose rates for samples in this investigation were determined from elemental concentrations of K, Rb, U, and Th by the method presented by Aitken (1998). Elemental analysis was obtained through instrumental neutron activation (INAA; Table A4.1). The collection depth and estimated average water content for each sample is also given in Table Ax. The cosmic ray dose at depth was calculated using the equations of Prescott and Hutton (1988, 1994).

Sample ID	depth (m)	H_2O (%)	K concentration (ppm)			Rb concentration (ppm)			Th concentration (ppm)			U concentration (ppm)		
GI1801	0.80	33 ± 3	15626	±	1532	48.09	±	4.46	3.979	±	0.363	0.991	±	0.088
GI1802	0.85	30 ± 3	16242	±	1574	47.89	±	4.43	4.358	±	0.397	1.290	±	0.107
GI1803	0.77	25 ± 5	13198	±	1263	34.98	±	3.67	10.869	±	0.981	3.021	±	0.221
GI1804	0.80	25 ± 5	14158	±	1320	46.46	±	4.61	3.126	±	0.287	1.158	±	0.101
GI1805	0.70	30 ± 3	10834	±	1109	35.42	±	3.79	5.371	±	0.488	2.001	±	0.151

Irradiations for INAA were performed at the Ohio State University Research reactor. INAA data reduction was carried out by Scientific Consulting Services, Dublin, OH.

Table A4.1. Dosimetrically relevent data. Elemental concentrations from instrumental neutron activation analysis (INAA).

The De distributions for all samples in this study were symmetric, having population mean to median ratios less than 1.05 (M/m in Table 1). The M/m ratio is a gauge of symmetry or asymmetry of the De data set. An M/m value of 1.00 is perfectly symmetric. M/m values greater than 1.00 are positively skewed, but value below 1.05 are considered an indicator of complete resetting of the OSL signal prior to deposition. Dispersion (sd/mean) is a gauge of the relative variance of the data set. The samples in this study exhibited very low dispersion with the exception of GI-3. Both independent data

sets from sample GI-3 gave the highest dispersion values, supporting the interpretation that the sediments at that location were disturbed (Table 1). Based on the observed parameters for the sample data sets, the mean and standard error of each equivalent dose distribution was used as the basis for age calculations. Ages, errors, and uncertainties are presented using the convention proposed in Lepper et al. (2011). See Table 4.1 in main text for the OSL age results and related data.

Interval	# Ridges	Age Range		Ridge Accumulation Rate (yr/ridge)		Average Accumulation Rate (yr/ridge)
		Max Range	Min Range	Max Rate	Min Rate	
GI-1 to GI-2	4	400-290	340-350	27.5	-2.5	12.5
GI-2 to GI-4	10.5	350-240	290-300	10.5	-0.9	4.8
GI-4 to GI-5	5.5	300-160	240-180	25.5	10	17.7
					Mean:	11.6

Table A4.2. Ridge accumulation rates. Age ranges calculated as follows: maximum range = age + error minimum range=age−error. Ridge accumulation rates calculated as follows: minimum ridge accumulation rate = (minimum age of older sample−maximum age of younger sample)/ridge count; maximum ridge accumulation rate = (maximum age of older sample−minimum age of younger sample)/ridge count.

4.3 Growth rate calculations

Progradation rates were determined by measuring the distance perpendicular to the strike of the ridge set to the shoreline and dividing that by the age difference between the earliest and the latest fully formed ridges (Table A4.1). Maximum, minimum and mean accretion rates were determined in order to give a feel for the uncertainty in the value that arises from uncertainty in the two OSL ages that are involved in each calculation (Table A4.1). In general, the calculated rates reflect maximum estimates given that potential gaps may exist in the sedimentary record due to possible hiatuses in sediment accumulation and/or erosive events.

Table A4.2 below shows calculations for the timeline of ridge set formation.

	Duration (yrs)	# ridges	Rate (yr/ridge)	Time (cumulative ybp)
Set 1	60	21	2.8	753
Set 2	60	14	4.3	693
Set 3	60	15	4.0	633
Set 4	75.5	5	15.1	574
Set 5	90.6	7	12.9	498
Set 6	75.5	5	15.1	407
Set 7	90.6	6	15.1	332
Set 8	90.6	6	15.1	241
Set 9	75.5	5	15.1	151
Set 10	75.5	5	15.1	75

Table A4.2. Timeline of ridge set formation using the average accumulation rate calculated in Table 4.1.

5. Comparison to other beach ridge systems

An attempt was made to compare the beach ridge geometry of Grand Isle to that of other locations (Table A5.1). Studies of 60 sandy, coastal beach ridge systems from around the world were compiled and the following information, when available, was entered into a database: beach ridge width, spacing, and amplitude; age range, width, and number of ridges in the system; average accretion rate and progradation rate. The average accretion rate refers to the number of years needed for one ridge and its associated swale to form, whereas the progradation rate is the rate of outward building measured in meters per year. Not all of this information was available for every study but some parameters could be deduced from those values that were available. In some studies, the beach ridge systems were divided into individual sets, each with their own characteristic geometric measurements, and these groupings were preserved. In a few cases, where beach ridge plain width was not provided the *Google Earth* measure tool was used to determine this value.

Location		Time to form (y)	Avg. Spacing (m) crest to crest	BRP Width (m)	# Ridges	Accretion Rate (ridges/yr)	Progradation Rate (m/yr)	Publication
Grand Isle, LA	I ▪	246	41.5	4000	50	0.203	16.26	Torres et al., 2019
	II ▪	574	101.8	7379	39	0.068	12.86	
Caminada Moreau, LA		420	47.14	*3300*	70	0.167	*7.86*	Penland et al., 1986
Richardson Hammock, FL		200	*22.5*	450	20	0.100	*2.25*	Rink & Lopez, 2010
Little St. George Island, FL	A	1400	*203.3*	3050	15	*0.011*	*2.18*	Rink & Lopez, 2010
	B	468	*200.0*	1200	6	*0.013*	*2.56*	
	C	1868	*202.4*	4250	21	*0.011*	*2.28*	
St. Joseph Peninsula, FL	A	250	*87.9*	615	7	*0.028*	*2.46*	Rink & Lopez, 2010
	B	350	*142.3*	2419	17	*0.049*	*6.91*	
St. Vincent Island, FL		1482	*72.2*	1300	18	*0.012*	*0.88*	Rink & Lopez, 2010
Cape San Blas, FL	A	300	*197.5*	1580	8	*0.027*	*5.27*	Rink & Lopez, 2010
	B	330	*186.7*	2800	15	*0.045*	*8.48*	
	C	630	*190.4*	4380	23	*0.037*	*6.95*	
Sanibel Island, FL		4300	*8.74*	**2360**	270	0.063	*1.82*	Missimer, 1973
Canaveral, FL	A	2140	100	2900	29	0.014	*1.36*	Rink & Forrest, 2005
	B	1730	148	2700	18	0.010	*1.56*	
	C	1730	80	2000	25	0.014	*1.16*	
Savannah River, GA		4500		10000			*2.22*	DePratter & Howard, 1977
Nayarit, Mexico		5000	42.4	10600	250	0.050	*2.2*	Curray et al., 1969
Tabasco, Mexico			*47*	**2800**	*59.6*			Psuty, 1965
Costa Rica		3900	*131.6*	2500	*19*	*0.005*	*0.641*	Nieuwenhuyse et al., 1994
Quadros Lagoon, Brazil			55	**1138**	21			Hesp et al., 2005
Santa Catarina, Brazil	Navegantes		20	5000			1	FitzGerald et al., 2007
	Pinheira	3000	25	5000	60		2	Hein et al., 2013
Golfo de Venezuela		4165	*86.7*	**6500**	75	*0.018*	1.56	Tanner, 1971
Boundary Bay, British Columbia		500		800			1.6	Engels & Roberts, 2005
		18		15.12			0.84	
		9		4.32			0.48	
Magdalen Islands, Canada	Les Sillons	1820		**700**	*13*	0.007	0.1	Remillard et al., 2015
Gulf of Almeria, Spain	H2	1200	*14.7*	*1000*	68	0.057	0.83	Goy et al., 2003
	H3	1200	*22.1*	*750*	34	0.028	0.625	
Rhone, France	Deladel	300		*3000*			10	Rey et al., 2009
	Peccais	100	*200*	*800*	4	0.040	8	
	Saint-Roman	120		983			8.2	
Danube Delta, Romania	Sacalin	45	80	600	*7.5*	*0.167*	*13.33*	Vespremeanu et al., 2016
	Buhaz	200	70	1200	*17.1*	*0.086*	*6*	
	Palade	240	70	500	*7.1*	*0.030*	*2.08*	
	West Saele	2200	40	1400	*35*	*0.016*	*0.64*	
	New Periteasca	200	50	800	*16*	*0.080*	*4.00*	
Samsø, Denmark		5000	*58.8*	1000	17	0.003	0.21	Hede et al., 2015
Northern Jutland, Denmark		1700			113	0.066	2	Nielsen et al., 2006
Flakket, Denmark	I	792	25	400	16	0.020	0.5	Clemmensen et al., 2012
	II	77	20	240	12	0.156	3.1	
	III	90	15	420	28	0.311	5.9	
Beachmere, NE Australia		560		*89.6*			0.16	Brooke et al., 2008 (a)
		940	*100*	*385*	3.9	0.004	0.41	
		90	23	*95.4*	*4.15*	*0.046*	1.06	
Burdekin Region, NE Australia		*5910*	65	6500	100	*0.017*	*1.10*	Belperio, 1983
Keppel Bay, NE Australia	6b	*100*		165			1.70	Brooke et al., 2008 (b)
	6a	*50*		215			4.30	
	3	*370*		625			1.70	
Moruya, SE Australia		*6830*	*33*	2000	60	0.009	0.27	Oliver et al., 2015
Guichen Bay, SE Australia	3	100	75	783	10.44	0.104	*7.83*	Bristow & Pucillo, 2006
	4	900	75	387	5.16	0.006	*0.43*	
	5	2600	75	1565	20.87	0.008	*0.60*	
LeFevre Pen., S Australia		5000		5000			*1*	Bowman & Harvey, 1986
Guichen Bay, S Australia		3900	75	3656	49	0.013	0.39	Murray-Wallace et al., 2002
Phra Thong, Thailand	Phase 1	1500		*3450*			2.3	Brill et al., 2015
	Phase 3	500		*1350*			2.7	
	Phase 4	1800		*1800*			1	
	Phase 6	800						
Kujukuri, Japan		6000		10			0.002	Tamura et al., 2008

Table A5.1. Table 5.1. The 60 sandy beach ridge systems used for comparison to Grand Isle. Underlined values are approximated based on a nearby BRP (Short, 1988). Italicized numbers are values that were derived, not directly provided by author. Bolded values are BRP widths obtained by measuring in Google Earth.

VITA

The author was born in Metairie, Louisiana. She obtained her bachelor's degrees in Earth & Environmental Sciences and Biology from the University of New Orleans in 2009 and 2011, respectively. After living in several states and working as a biologist in the Florida Everglades, she returned to University of New Orleans in 2016 to enroll in the Earth & Environmental Sciences graduate program to pursue a M.S. degree in coastal and geomorphologic studies under Dr. Mark Kulp.